Biophysical Journal
Article

Biophysical Society

SF1 Phosphorylation Enhances Specific Binding to U2AF^{65} and Reduces Binding to 3′-Splice-Site RNA

Rakesh Chatrikhi,[1] Wenhua Wang,[1] Ankit Gupta,[1] Sarah Loerch,[1] Alexandre Maucuer,[2] and Clara L. Kielkopf[1,*]
[1]Department of Biochemistry and Biophysics, University of Rochester School of Medicine, Rochester, New York; and [2]Université d'Evry-Val-d'Essonne, Evry Cedex, France

ABSTRACT Splicing factor 1 (SF1) recognizes 3′ splice sites of the major class of introns as a ternary complex with U2AF^{65} and U2AF^{35} splicing factors. A conserved SPSP motif in a coiled-coil domain of SF1 is highly phosphorylated in proliferating human cells and is required for cell proliferation. The UHM kinase 1 (UHMK1), also called KIS, double-phosphorylates both serines of this SF1 motif. Here, we use isothermal titration calorimetry to demonstrate that UHMK1 phosphorylation of the SF1 SPSP motif slightly enhances specific binding of phospho-SF1 to its cognate U2AF^{65} protein partner. Conversely, quantitative fluorescence anisotropy RNA binding assays and isothermal titration calorimetry experiments establish that double-SPSP phosphorylation reduces phospho-SF1 and phospho-SF1–U2AF^{65} binding affinities for either optimal or suboptimal splice-site RNAs. Domain-substitution and mutagenesis experiments further demonstrate that arginines surrounding the phosphorylated SF1 loop are required for cooperative 3′ splice site recognition by the SF1-U2AF^{65} complex (where cooperativity is defined as a nonadditive increase in RNA binding by the protein complex relative to the individual proteins). In the context of local, intracellular concentrations, the subtle effects of SF1 phosphorylation on its associations with U2AF^{65} and splice-site RNAs are likely to influence pre-mRNA splicing. However, considering roles for SF1 in pre-mRNA retention and transcriptional repression, as well as in splicing, future comprehensive investigations are needed to fully explain the requirement for SF1 SPSP phosphorylation in proliferating human cells.

INTRODUCTION

Expression of splicing factor 1 (SF1, also called ZFM1) is required for viability in yeast, flies, nematodes, and human cell lines (1–4), and the SF1 gene locus is tightly linked to multiple endocrine neoplasia type I (5). SF1 associates with U2 small nuclear ribonucleoprotein (snRNP) auxiliary factor subunits (U2AF^{65} and U2AF^{35}, also called U2AF2 and U2AF1) (1,6,7). Like SF1, the U2AF^{65} and U2AF^{35} splicing factors are essential for viability in multicellular eukaryotes (e.g., (8,9).), and the U2AF^{35} subunit is frequently mutated in myelodysplastic syndromes (10–12). The ternary complex comprising the SF1 and U2AF subunits recognizes consensus pre-mRNA signals in the early stages of pre-mRNA splicing (reviewed in (13)) (Fig. 1 *A*). Specifically, a K-homology-quaking motif (KH-QUA2) of SF1, RNA recognition motifs (RRMs) of U2AF^{65}, and zinc knuckles of U2AF^{35} recognize the branch-point sequence (BPS), polypyrimidine (Py) tract, and intron-exon junction of the major class of 3′ splice sites (14–18) (Fig. 1 *B*). The yeast homolog of SF1 also has been implicated in cross talk with the U1 snRNP (1,19–21). Subsequently, ATP-dependent association of the U2 snRNP with the pre-mRNA displaces the SF1 subunit; instead, an SF3b155 subunit (also called SF3B1) of the U2 snRNP interacts with the U2AF^{65} subunit of the U2AF heterodimer (22–25).

The importance of the U2AF subunits for spliceosome assembly in mammals has been firmly established by biochemical reconstitution experiments (e.g., (15,16), among others). In contrast, SF1 selectively regulates splicing of a subset of introns (26–29). One possible explanation is a transient role and rapid recycling of SF1 (30,31), such that trace amounts are sufficient to support splicing of traditional pre-mRNA substrates. Yet a direct relationship between the selective role for SF1 in pre-mRNA splicing and its requirement for cell viability is uncertain. Indeed, SF1 has been implicated in other major steps of gene expression, including nuclear pre-mRNA retention (2) and transcriptional repression (32,33). The association of SF1 and

Submitted July 28, 2016, and accepted for publication November 8, 2016.

*Correspondence: clara_kielkopf@urmc.rochester.edu

Wenhua Wang's present address is Bristol-Myers Squibb, New Brunswick, New Jersey.

Ankit Gupta's present address is NYU Langone Medical Center, New York, New York.

Editor: James Cole.

http://dx.doi.org/10.1016/j.bpj.2016.11.007

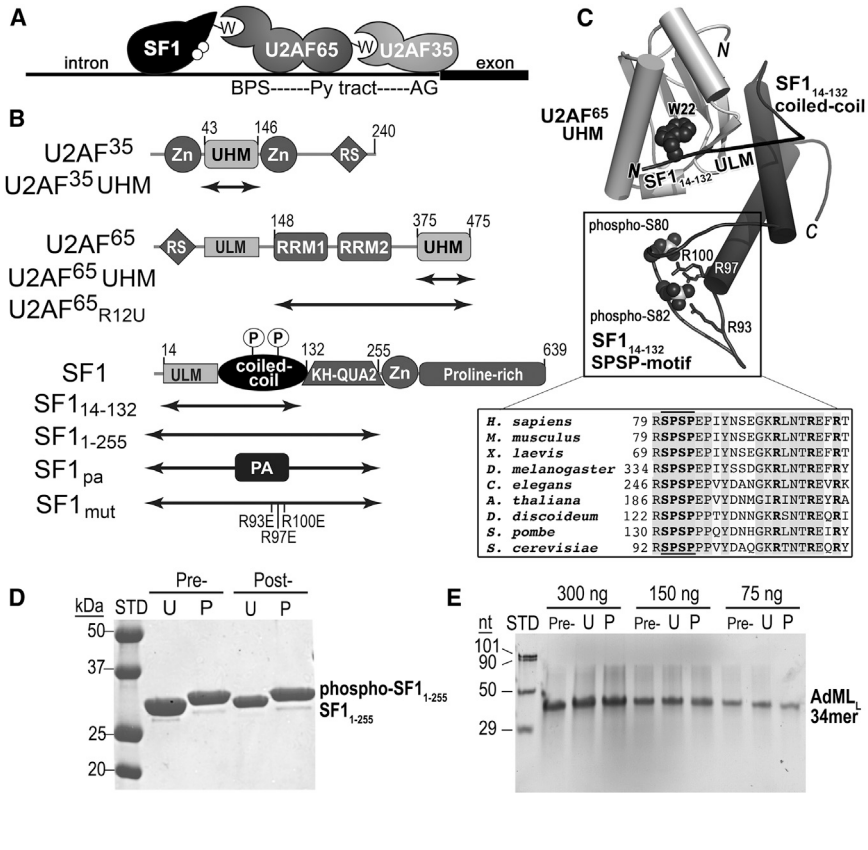

FIGURE 1 SF1 structure and function in pre-mRNA splicing. (*A*) Schematic diagram of the early-stage SF1-U2AF^{65}-U2AF^{35} splicing-factor complex recognizing the 3′ splice site. ULMs are represented by "W." White circles represent UHMK1-phosphorylation sites. BPS, branch point sequence; Py, polypyrimidine. (*B*) Domains of SF1, U2AF^{65}, and U2AF^{35} splicing factors. The boundaries of constructs used in this study are indicated by double-headed arrows. Zn, CCCH zinc knuckle; UHM, U2AF homology motif; ULM, U2AF ligand motif; RRM, RNA recognition motif, RS, arginine-serine repeat; KH-QUA2, K homology with quaking-2 motif; PA, protein A; circled P, UHMK1-phosphorylation sites. (*C*) Structure of the phosphorylated SF1$_{14–132}$-U2AF^{65} UHM complex (PDB: 4FXW). A line representing residues that are absent from the electron density connects the C-terminus of the ULM to the coiled-coil motifs. The tryptophan of the ULM (W22) and phosphorylated serines are shown as spheres and arginine residues that are mutated in this study are shown in stick representation. The inset shows a sequence alignment of the UHMK1-phosphorylated SPSP motif (*bold* (between lines)). (*D* and *E*) Samples of (*D*) phospho-SF1$_{1–255}$ and (*E*) AdML$_L$ RNA under experimental conditions. Samples either before (*Pre-*) or after (*Post-*) incubating at 23°C for 2 h in the presence of a 10-fold excess of SF1 (U) or phospho-SF1 (P) were analyzed by denaturing gel electrophoresis and stained using (*D*) Coomassie blue or (*E*) SYBR Gold, respectively. The phosphorylated form of SF1$_{1–255}$ runs higher by SDS-PAGE. STD, size markers; nt; nucleotides. Conditions were identical to those of fluorescence assays with the exception that the RNase inhibitor Superase-In (Ambion, Life Technologies) was omitted here to fully rule out RNase contamination.

U2AF in extra-spliceosomal complexes (6) and the involvement of U2AF^{65} in the nuclear pre-mRNA retention activity of SF1 (34–36) suggest that the SF1-U2AF^{65} complex contributes to these multiple SF1 functions.

The protein-protein interaction domains mediating the SF1-U2AF^{65}-U2AF^{35} complex are called "U2AF homology motifs" (UHMs) based on their original discovery in the U2AF^{65} and U2AF^{35} prototypes (37,38). The UHM shares the core topology of the RRM fold, yet the ribonucleoprotein consensus motifs (RNPs) diverge from typical RRM residues and have lost the ability to bind RNA (reviewed in (39)). Instead, an acidic α-helix and hydrophobic pocket of the UHM recognize basic residues and a tryptophan residue of a peptide ligand, called a "U2AF ligand motif" (ULM). Sequence searches extrapolating from the U2AF^{65} and U2AF^{35} UHMs identified putative UHMs in several nuclear proteins, many of which have now been confirmed to bind ULMs (e.g., (40,41)). The ULMs share similar short, linear epitopes of positively charged and tryptophan amino acids, yet only a handful of ULM-containing proteins have been confirmed to date, and their interaction partners are remarkably specific. For example, the SF1 ULM targets the U2AF^{65} UHM, which also sequentially associates with an SF3b155 ULM, whereas the U2AF^{65} ULM mediates the heterodimer with the U2AF^{35} UHM. As such, the means for limiting off-target cross talk among UHMs and ULMs presents a molecular conundrum.

Extensions of the core ULM sequence offer one means to increase the interface, and hence specificity, of UHM-ULM complexes. For the U2AF^{35} UHM-U2AF^{65} ULM prototype, a proline-rich region at the C-terminus of the U2AF^{65} ULM sandwiches an otherwise exposed tryptophan side chain of the U2AF^{35} UHM (38). For SF1, a coiled-coil domain at the C-terminus of the SF1 ULM extends its interface with the U2AF^{65} UHM (42,43) (Fig. 1 *C*). Despite extensive hydrophobic and electrostatic contacts, the SF1 coiled coil makes subtle contributions to the affinity of the SF1-U2AF^{65} complex (43). However, whether this SF1 coiled coil could discriminate against the SF1 ULM binding off-target UHMs remains unknown.

Phosphorylation within or adjacent to ULMs is a second mechanism for regulating the specificity of UHM interactions. In perhaps the earliest example of phosphorylation-sensitive ULM-UHM interactions, phosphorylation of a serine in the SF1 ULM by cGMP-dependent protein kinase I was shown to reduce SF1 association with U2AF^{65} (44). In a second, more recent example, phosphorylation near a ULM of ataxin-1 (ATX1) was found to promote its

binding to the 14-3-3 protein, which in turn out-competes ATX1 association with the U2AF^{65} UHM (45).

SF1 also is phosphorylated on a conserved SPSP motif within its coiled-coil domain (46) (Fig. 1 *C*, *inset*). Both serines in the SPSP motif (S80 and S82) of endogenous SF1 isolated from proliferating cells are highly phosphorylated. Mutation of both serines in the SF1 SPSP motif to phosphorylation-resistant alanines significantly reduces NIH 3T3 cell proliferation (42) and leads to massive splicing changes in fission yeast strains (47). The SF1 SPSP motif is likely to be a substrate for several kinases. A UHM-containing kinase (UHMK1, also called KIS) highly phosphorylates both S80 and S82 of this SF1 motif (46). Yet, the SPSP-containing region of SF1 remains phosphorylated in more than half of the detected SF1 proteins in UHMK1-knockout mice (48), which suggests that other kinases regulate this SF1 motif. For example, SRPK2 detectably phosphorylates the second serine (S82) of the SF1 SPSP motif in vitro, and could act to phosphorylate SF1 in vivo (47). Accordingly, UHMK1 is differentially expressed in the brain (48) and may serve specific roles in the nervous system.

The functions of SF1 SPSP motif phosphorylation remain largely mysterious. Structurally, phosphorylation of the SF1 SPSP motif induces local folding of an arginine "claw" (R93, R97, and R100) surrounding the phosphorylated serines (42,43). One hypothesis is that this structural change augments the SF1 ULM by promoting formation of the coiled-coil interface of SF1 with the U2AF^{65} UHM. Accordingly, the UHMK1-phosphorylated SPSP motif subtly promotes SF1 binding to U2AF^{65} in pull-down assays (46,49). Although little phosphorylation-dependent increase in SF1 binding U2AF^{65} had been observed by isothermal titration calorimetry (ITC) (43), we were concerned that use of a phosphate-containing buffer could have reduced a potential response. Moreover, despite these studies of phosphorylated SF1 interactions with U2AF^{65}, whether SPSP phosphorylation of SF1 could discriminate against noncognate binding to other UHMs was unknown. For association with 3′ splice sites, electrophoretic mobility shift assays (EMSAs) of SF1 in the presence of SRPK2 suggested that S82 phosphorylation slightly increased SF1 binding to RNAs containing suboptimal BPSs (47). However, SRPK2 preferentially phosphorylates S82 rather than both serines of the SPSP motif, and the EMSA is not an equilibrium method due to separation of the ligand and macromolecule during electrophoresis.

Here, we use ITC and fluorescence anisotropy RNA binding assays to measure the influence of SPSP phosphorylation on SF1 interactions with UHM-containing proteins and 3′-splice-site RNA. Altogether, SPSP phosphorylation subtly enhances the specificity of SF1 for binding the cognate U2AF^{65} UHM and discriminates against off-target UHMs. By either ITC or fluorescence-based RNA binding assays, phosphorylation of the SPSP motif slightly decreases the affinity of SF1 for splice-site RNAs. Domain substitution and mutagenesis further implicate arginines surrounding the phosphorylated motif as sites of SF1-RNA interactions, which could explain the discontinuous spacing of the BPS and Py tract consensus signals at the 3′ splice site. The reproducible effects of SPSP phosphorylation on SF1 binding to UHM-containing proteins and splice-site RNAs are likely to contribute to SF1 function. However, alternative functions may contribute to the significantly reduced proliferation of human cells in the presence of the SF1 APAP mutation (42).

MATERIALS AND METHODS

Protein expression and purification

All proteins are the human homologs expressed as glutathione-*S*-transferase (GST) fusions in *Escherichia coli* using either pGEX-6p or an in-house pGEX variant encoding a TEV protease site. The nomenclature and boundaries of the SF1 (NCBI RefSeq: NP_004621) and U2AF^{65} (NCBI RefSeq: NP_009210) protein expression constructs used in this study are given in Fig. 1 *B*. Other recombinant proteins include the UHM domains of U2AF^{35} (residues 43–146 of NCBI RefSeq: NP_006749), CAPERα (residues 411–524 of NCBI RefSeq: NP_004893), and SPF45 (residues 301–401 of NCBI RefSeq: NP_116294). After an initial glutathione affinity step, we cleaved the GST-tags during overnight dialysis using PreScission Protease for SF1 and U2AF^{65} proteins and TEV protease for the U2AF^{35} UHM, CAPERα UHM, and SPF45 UHM. The splicing-factor proteins were further purified by subtractive GST-affinity chromatography followed by anion- or cation-exchange chromatography. Purified SF1 proteins were phosphorylated by UHMK1 under conditions similar to those described in (42,50) and then separated from UHMK1 by size-exclusion chromatography. The phosphorylation of the SF1 protein appears complete as judged by a characteristic shift by sodium dodecyl sulfate polyacrylamide gel electrophoresis (SDS-PAGE) (42,46) (Fig. 1 *D*). The complexes of SF1 variants with U2AF^{65} were prepared by mixing 1:1 molar ratios of the separately purified subunits followed by size-exclusion chromatography. All proteins used for RNA binding experiments, as well as phosphorylated SF1 or phospho/unphospho-SF1-U2AF^{65} complexes, were finally purified by size-exclusion chromatography using a HiLoad 16/600 Superdex 75 pg (GE Healthcare, Little Chalfont, United Kingdom) in 100 mM NaCl, 25 mM HEPES buffer (pH 7.4), and 0.2 mM TCEP buffer. Phospho-SF1$_{1–255}$-U2AF$^{65}{}_{R12U}$, SF1pa-U2AF$^{65}{}_{R12U}$, and SF1mut-U2AF$^{65}{}_{R12U}$ showed no detectable difference in complex formation from unmodified SF1$_{1–255}$-U2AF$^{65}{}_{R12U}$ by size-exclusion chromatography at ~5 μM concentrations.

ITC methods

Protein samples for ITC were dialyzed against a >200-fold greater volume of 25 mM HEPES (pH 7.4), 0.2 mM TCEP, and either the indicated concentration of NaCl for U2AF^{65} titration into SF1 (Table S1 in the Supporting Material), 50 mM NaCl for off-target UHM titrations (Table 1), or 100 mM NaCl for RNA titrations (Tables 2 and 3). A control titration of B3P3$_{SUBOPT}$ RNA into SF1mut-U2AF$^{65}{}_{R12U}$ in 100 mM NaCl and 25 mM sodium phosphate (pH 7.4) was compared to the HEPES buffer (Table 3; Fig. S6). The synthetic B3P3$_{SUBOPT}$ RNA of sequence 5′-UGGUAAC UUUCUCUUUCUCUCUCCC (branch site underlined) was deprotected and desalted according to manufacturer instructions (Dharmacon, GE Healthcare). The RNA was resuspended in water and diluted >50-fold in dialysis buffer. Proteins or RNA at the concentrations indicated in Figs. 2, 4, 6, 7, 8, S1, S2, and S4–S6 were titrated at 30°C with 4 min of relaxation time between injections using a VP-ITC

TABLE 1 Thermodynamics of U2AF Homology Motifs binding SF1 or Phospho-SF1

Interaction[a]	K_D (nM)	ΔG[b] (kcal mol^{-1})	ΔH (kcal mol^{-1})	$-T\Delta S$[c] (kcal mol^{-1})	n[d]
$U2AF^{65}$ UHM Titrated into[e]					
$SF1_{14–132}$	43 ± 1	−10.2 ± 0.1	−13.5 ± 0.1	3.3 ± 0.1	1.0 ± 0.1
Phospho-$SF1_{14–132}$	24 ± 1	−10.6 ± 0.1	−20.6 ± 0.1	10.0 ± 0.1	0.9 ± 0.1
SPF45 UHM Titrated into[f]					
$SF1_{14–132}$	99 ± 2	−9.7 ± 0.1	−15.2 ± 0.2	5.5 ± 0.2	1.0 ± 0.1
Phospho-$SF1_{14–132}$	170 ± 8	−9.4 ± 0.1	−14.5 ± 0.1	5.1 ± 0.1	1.1 ± 0.1
$U2AF^{35}$ UHM Titrated into[f]					
$SF1_{14–132}$	2430 ± 350	−7.8 ± 0.1	−30.9 ± 1.2	23.1 ± 1.3	1.0 ± 0.1
Phospho-$SF1_{14–132}$	3540 ± 1140	−7.6 ± 0.2	−38.2 ± 2.3	30.6 ± 2.1	0.9 ± 0.1
CAPERα UHM Titrated into[f,g]					
$SF1_{14–132}$[h]	11,000 ± 700	−6.9 ± 0.1	−11.5 ± 0.2	4.6 ± 0.2	1.0 ± 0.1
Phospho-$SF1_{14–132}$	57,000 ± 42,000	−6.0 ± 0.5	−18.3 ± 11.4	12.3 ± 11.8	1.0 ± 0.3

[a]Values are expressed as the mean ± SD of at least two independent titrations.
[b]ΔG values were calculated using the equation $\Delta G = -RT \ln (K_D^{-1})$ at T = 303 K.
[c]$-T\Delta S$ values were calculated using the equation $-T\Delta S = \Delta G - \Delta H$.
[d]Apparent stoichiometry of UHM/SF1 proteins.
[e]Proteins in 100 mM NaCl, 25 mM HEPES (pH 7.4), and 0.2 mM TCEP.
[f]Proteins in 50 mM NaCl, 25 mM HEPES (pH 7.4), and 0.2 mM TCEP.
[g]Values for phospho-SF1 binding CAPERα UHM are estimates due to the very low c-value of 1.
[h]Values for $SF1_{14-132}$ binding CAPERα UHM are from Loerch et al. (40).

(GE Healthcare). Control titrations of SPF45 UHM, $U2AF^{35}$ UHM, $SF1_{1–255}$-$U2AF^{65}{}_{R12U}$ complex, or $B3P3_{SUBOPT}$ RNA into buffer (Fig. S1) were linear and showed negligible heats of dilution. The CAPERα UHM titration into buffer is shown in (40). The average heats of the $U2AF^{35}$ or CAPERα UHM dilution (Fig. S1 *B* and (40)) were used to correct the relatively low-affinity isotherms of these UHMs titrated into $SF1_{14-132}$ or phospho-$SF1_{14-132}$ (Fig. 2, *E–G*). All other isotherms were corrected for heats of dilution using an average of four to five data points at the saturated plateau of the titration. The isotherms were fit using Origin v7.0 (MicroCal, Northampton, MA). The average values and standard deviations of the tables and figures result from at least two independent titration experiments. The phosphorylated state of SF1 was stable throughout the ITC experiments (Fig. 1 *D*) and RNA oligonucleotide lacked detectable ribonuclease activity (Fig. 1 *E*). The c-values of the isotherms (where $c = K_A \times [M]$, M is the macromolecule in the sample cell, and the stoichiometry is assumed to be 1) are given in the figure legends. A c-value between ~5 and 500 is considered reliable for K_D and n (apparent stoichiometry) measurement. Enthalpy changes may still be determined from isotherms with higher c-values (51).

Fluorescence anisotropy RNA binding assay

Synthetic RNAs with 5′-fluorescein (Fl) labels (Dharmacon, GE Healthcare) were deprotected and desalted according to manufacturer instructions and used without further purification. RNA sequences used for fluorescence measurements included $AdML_S$ 5′-UACUU**A**UCCUGUCC CUUUUUUUUC, $AdML_L$ 5′-UUCGUGCUG**A**CCCUGUCCCUUUUUU UUCCACAGC, or BPS_{SUBOPT} 5′-GAGUCAGACUA**A**CUCGUUGUU UAG (branch site underlined). Fluorescence anisotropy changes during titration of 25 nM RNA with the indicated final concentrations of protein (Figs. 3 and 5) in a water-thermostatted cuvette at 23°C using a FluoroMax-3 spectrophotometer (HORIBA Jobin Yvon, Kyoto, Japan) were measured and analyzed in a manner similar to that described in (52,53). Both macromolecules were diluted >50-fold in 150 mM NaCl, 25 mM HEPES (pH 7.4), 0.2 mM TCEP, and 0.1 U μL^{-1} Superase-In (Ambion, Life Technologies, Carlsbad, CA). Samples were excited at 490 nm and emission intensities were recorded at 520 nM with a slit width of 5 nm. Data were fit by non-linear regression assuming single-site binding to obtain the apparent equilibrium dissociation constant (K_D) using the equation below, where X is the total protein concentration, [RNA] is the total RNA concentration, r is the observed anisotropy at the ith titration, r_B is the anisotropy at zero protein concentration, and r_F is the anisotropy at saturating protein concentration (floated in fit):

$$r = r_F + \frac{r_B - r_F}{2[RNA]}\left(K_D + X + [RNA]\right) - \sqrt{\left(K_D + X + [RNA]\right)^2 - (4[RNA]X)}$$

The K_A was calculated using the relationship K_D^{-1}.

TABLE 2 Thermodynamics of Splicing Factor Subunits Binding B3P3-Splice Site RNA

B3P3 RNA Titrated into[a]	K_D (nM)	ΔG[b] (kcal mol^{-1})	ΔH (kcal mol^{-1})	$-T\Delta S$[c] (kcal mol^{-1})	n[d]
$U2AF^{65}{}_{R12U}$	509 ± 4	−8.8 ± 0.1	−52.1 ± 0.1	43.3 ± 0.1	0.8 ± 0.1
$SF1_{1–255}$	40 ± 1	−10.3 ± 0.1	−23.3 ± 0.1	13.0 ± 0.1	0.9 ± 0.1
Phospho-$SF1_{1–255}$	78 ± 9	−9.8 ± 0.1	−20.9 ± 0.1	11.1 ± 0.1	1.0 ± 0.1
$SF1_{PA}$	114 ± 11	−9.7 ± 0.1	−20.9 ± 0.1	11.2 ± 0.1	1.0 ± 0.1
SF1mut	186 ± 30	−9.3 ± 0.1	−20.0 ± 0.1	10.7 ± 0.1	1.0 ± 0.1

[a]Values are expressed as the mean ± SD of at least two independent titrations.
[b]ΔG values were calculated using the equation $\Delta G = -RT \ln (K_A)$, where T = 303 K.
[c]$-T\Delta S$ values were calculated using the equation $-T\Delta S = \Delta G - \Delta H$.
[d]Fits are "ligand-in-cell" such that "n" is the apparent stoichiometry of protein/RNA.

TABLE 3 Thermodynamics of Splicing Factor Complexes Binding B3P3-Splice Site RNA

Interaction:[a]	K_D (nM)	ΔG[b] (kcal mol^{-1})	ΔH (kcal mol^{-1})	$-T\Delta S$[c] (kcal mol^{-1})	n[d]
B3P3 RNA Titrated into Splicing-Factor Complexes					
$SF1_{1–255}$-$U2AF^{65}{}_{R12U}$, site 1	2 ± 1	−12.1 ± 0.1	−60.1 ± 0.1	47.9 ± 0.1	0.8 ± 0.1
$SF1_{1–255}$-$U2AF^{65}{}_{R12U}$, site 2	500 ± 10	−8.7 ± 0.1	−65.3 ± 0.1	56.6 ± 0.1	0.3 ± 0.1
Phospho-$SF1_{1–255}$-$U2AF^{65}{}_{R12U}$, site 1	7 ± 5	−11.5 ± 0.1	−60.4 ± 0.1	48.9 ± 0.1	0.8 ± 0.1
Phospho-$SF1_{1–255}$-$U2AF^{65}{}_{R12U}$, site 2	600 ± 80	−8.7 ± 0.1	−65.3 ± 0.1	57.6 ± 0.1	0.4 ± 0.1
SF1pa-$U2AF^{65}{}_{R12U}$	85 ± 1	−9.8 ± 0.1	−67.5 ± 0.1	57.7 ± 0.1	0.9 ± 0.1
SF1mut-$U2AF^{65}{}_{R12U}$	82 ± 1	−9.8 ± 0.1	−76.7 ± 0.1	66.9 ± 0.1	0.9 ± 0.1
SF1mut-$U2AF^{65}{}_{R12U}$[e]	104 ± 7	−9.7 ± 0.2	−68.4 ± 0.2	58.6 ± 0.2	1.0 ± 0.1
Splicing-Factor Complexes Titrated into B3P3 RNA[f]					
$SF1_{1–255}$-$U2AF^{65}{}_{R12U}$, site 1 (reverse)	160 ± 80	−9.5 ± 0.1	−22.3 ± 0.1	12.8 ± 0.1	0.6 ± 0.1
$SF1_{1–255}$-$U2AF^{65}{}_{R12U}$, site 2 (reverse)	7 ± 1	−11.3 ± 0.1	−53.2 ± 0.1	42.0 ± 0.1	0.9 ± 0.2
Phospho-$SF1_{1–255}$-$U2AF^{65}{}_{R12U}$, site 2 (reverse)	115 ± 5	−9.8 ± 0.1	−81.1 ± 4.9	71.4 ± 4.9	0.5 ± 0.1
Phospho-$SF1_{1–255}$-$U2AF^{65}{}_{R12U}$, site 1 (reverse)	18 ± 3	−10.8 ± 0.1	−36.2 ± 4.5	25.5 ± 4.7	0.7 ± 0.2

[a]Values are expressed as the mean ± SD of at least two independent titrations.
[b]ΔG values were calculated using the equation $\Delta G = -RT \ln (K_A)$ where T=303 K
[c]$-T\Delta S$ values were calculated using the equation $-T\Delta S = \Delta G - \Delta H$.
[d]Fits are "ligand-in-cell" such that "n" is the apparent stoichiometry of protein/RNA.
[e]Dialyzed into 100 mM NaCl and 25 mM sodium phosphate buffer (pH 7.4). Macromolecules for other experiments in this table were in 100 mM NaCl, 25 mM HEPES (pH 7.4).
[f]Apparent stoichiometry of protein/RNA (n).

Statistical significance of results

We observe small differences between binding constants of the phosphorylated and those of the unmodified SF1 for UHM-containing proteins or RNA. These differences are reproducible in at least two ITC experiments with distinct protein preparations and at least triplicate technical replicates of fluorescence anisotropy RNA binding assays, which are customary sample sizes with the power to detect significant differences, if present. In Figs. 2, *H* and *I*, 3, 4 *D*, 5, 6, *D* and *E*, 7 *D*, and 8 *D*, we plot the K_A values in a bar graph and provide the results of unpaired two-tailed t-tests with Welch's correction as *$p < 0.05$, **$p < 0.005$. The t-test is robust and can withstand violations of model assumptions (e.g., (54)). However, the t-test assumes a normally distributed population that differs from the small number of replicates here and should be considered here only as a starting point for critical assessment.

RESULTS

UHMK1 phosphorylation slightly enhances SF1 affinity for U2AF^{65}

Originally, pull-down experiments showed that phosphorylation of the SF1 SPSP motif by UHMK1 increased retention of full-length $U2AF^{65}$ by ~2-fold (46). However, the affinities of SF1 (residues 1–260) and UHMK1-phosphorylated (phospho-) SF1 for a $U2AF^{65}$ fragment comprising two central RRMs and the C-terminal UHM ($U2AF^{65}{}_{R12U}$, residues 148–475) appeared similar when measured by ITC in a phosphate-containing buffer (20 mM sodium phosphate (pH 6.5) and 50 mM NaCl) (43). To rule out competitive binding or possible allosteric effects of phosphate ions via the SF1 phosphorylation sites, we used ITC to measure the affinities of unmodified and phospho-$SF1_{1–255}$ (residues 1–255) for $U2AF^{65}{}_{R12U}$ in 25 mM HEPES buffer (pH 7.4), 100 mM NaCl (Fig. S2, *A* and *B*). We used UHMK1 to phosphorylate the $SF1_{1–255}$ protein in a method identical to that used for our prior crystal structure (42), and the similar shift by SDS-PAGE suggests that both serines of the motif are phosphorylated as seen in our crystal structure. This phosphorylated state was stable under the conditions of the binding experiments (Fig. 1 *D*).

Similar to the ITC in phosphate buffer described in a previous study (43), UHMK1 phosphorylation increased the binding affinity of $SF1_{1–255}$ for $U2AF^{65}{}_{R12U}$ by <2-fold (Table S1). We compared the affinity of a minimal $U2AF^{65}$ UHM for an SF1 construct that included the ULM and coiled coil but lacked the RNA binding domain (residues 14–132, $SF1_{14-132}$) (Fig. 2, *A* and *B*). We observed a subtle enhancement after UHMK1 phosphorylation of phospho-$SF1_{14–132}$ binding to the $U2AF^{65}$ UHM similar to that observed for the longer constructs (Table S1). Comparison of the $SF1_{1-255}$-$U2AF^{65}{}_{R12U}$ and $SF1_{14-132}$-$U2AF^{65}$ UHM affinities indicated that the SF1 and $U2AF^{65}$ RNA binding domains make little contribution to, and even slightly interfere with (by twofold), formation of the SF1-$U2AF^{65}$ complex.

Since these SF1-$U2AF^{65}$ binding affinities were relatively high for reliable measurement by ITC (c-values of 100–230), we repeated the unmodified and phospho-$SF1_{14–132}$-$U2AF^{65}$ UHM ITC at a higher salt concentration (25 mM HEPES (pH 7.4) and 250 mM NaCl) to reduce the slope (and hence improve the fits) of the isotherms (c-values of 16 and 24 for unmodified and phospho-$SF1_{14–132}$ in Fig. S2, *C* and *D*, respectively). As expected, the higher ionic strength conditions reduced the affinities of the $SF1_{14–132}$ or phospho-$SF1_{14–132}$ complexes with the $U2AF^{65}$ UHM (Table S1),

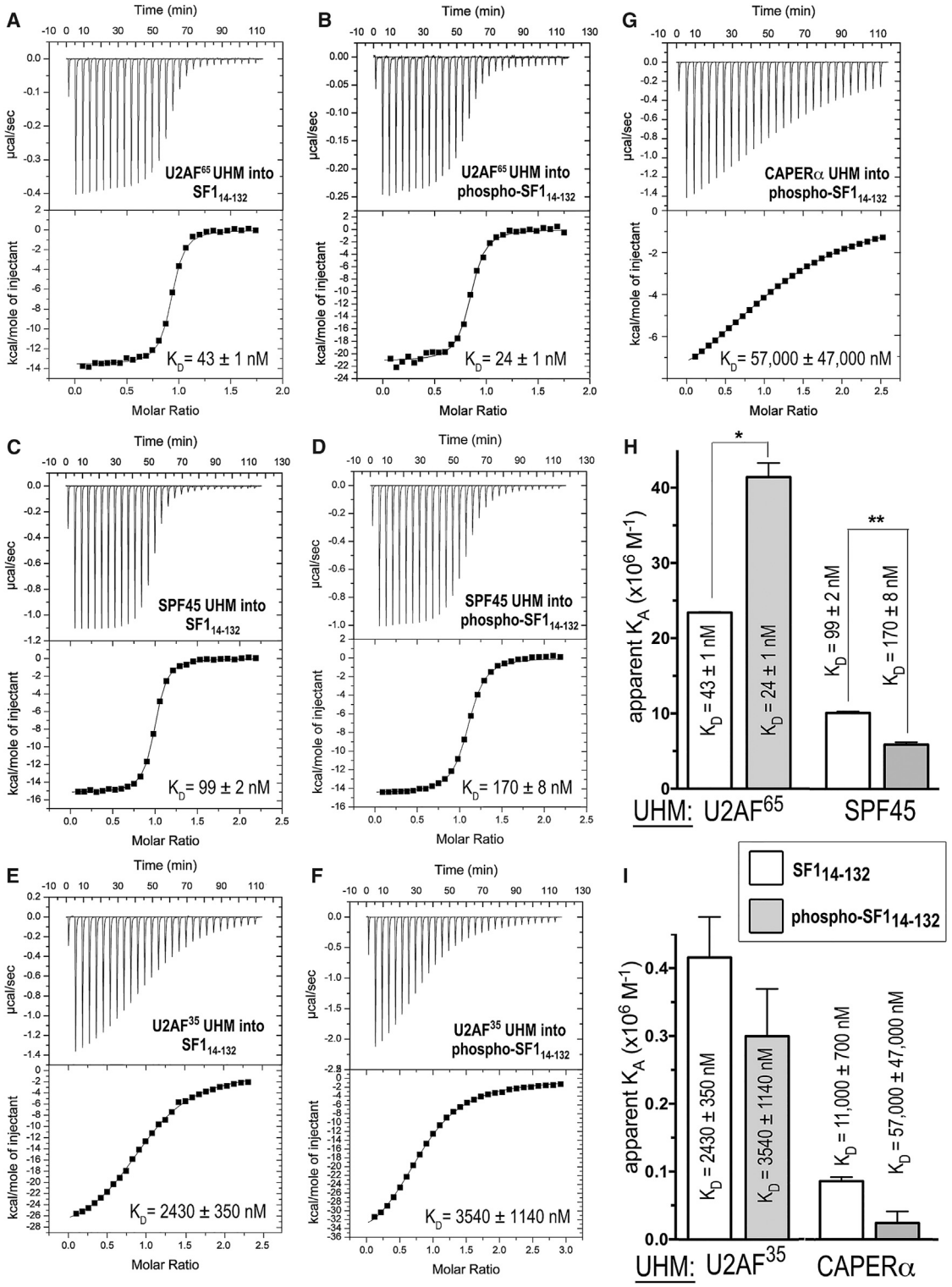

FIGURE 2 ITC results for $SF1_{14–132}$ or phospho-$SF1_{14–132}$ titrated with UHM proteins. (*A–G*) Representative isotherms fit with identical sites models. Titrations were of (*A*) 90 μM $U2AF^{65}$ UHM into 10 μM $SF1_{14-132}$, c = 230; (*B*) 32 μM $U2AF^{65}$ UHM into 4 μM phospho-$SF1_{14–132}$, c = 170; (*C*) 200 μM SPF45 UHM into 20 μM $SF1_{14–132}$, c = 200; (*D*) 200 μM SPF45 UHM into 20 μM phospho-$SF1_{14–132}$, c = 120; (*E*) 200 μM $U2AF^{35}$ UHM into 20 μM $SF1_{14-132}$, c = 8; (*F*) 260 μM $U2AF^{35}$ UHM into 20 μM phospho-$SF1_{14–132}$, c = 6; and (*G*) 600 μM CAPERα UHM into 50 μM phospho-$SF1_{14–132}$, c = 1. (*H* and *I*) Bar graphs showing the apparent equilibrium affinities (K_A) of $SF1_{14–132}$ (*white bars*) and phospho-$SF1_{14–132}$ (*gray bars*) for the indicated UHM proteins. The apparent equilibrium dissociation constants ($K_D = K_A^{-1}$) and the standard deviations of at least two replicates are given. Values from (*G*) are estimates due to the low affinity binding, which is at the limit for reliable fits of ITC data.

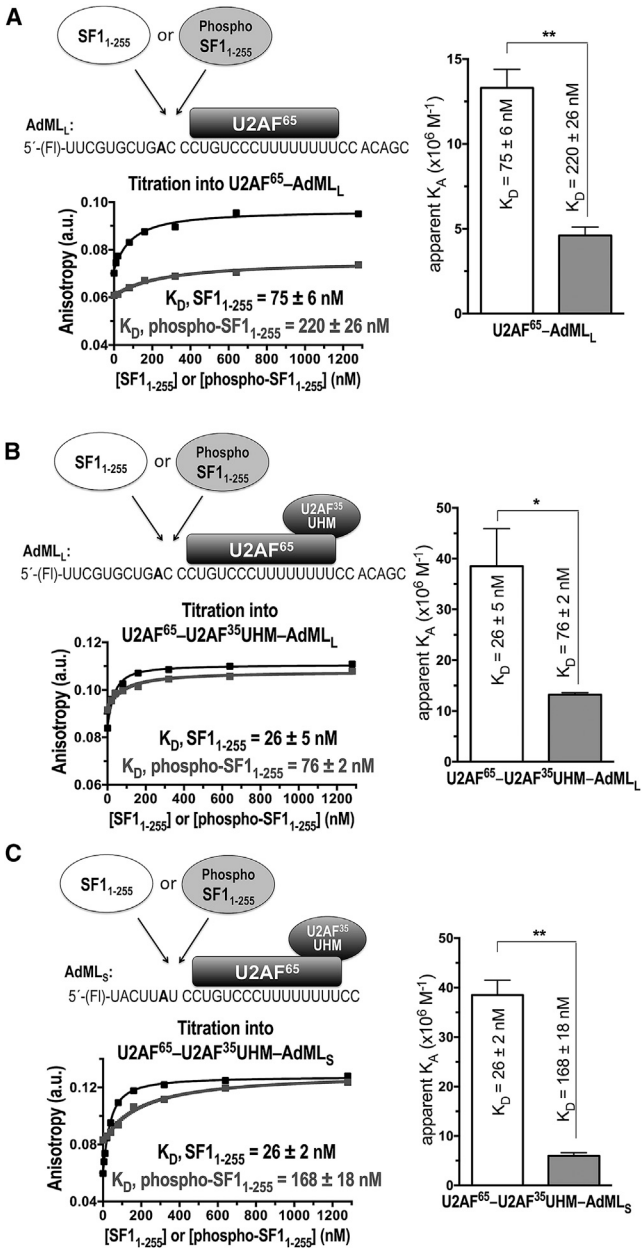

FIGURE 3 Fluorescence anisotropy RNA binding assay of $SF1_{1–255}$ (*white bars*, *black binding curve*) or phospho-$SF1_{1-255}$ (*gray shading and binding curve*) proteins titrated into fluorescein (Fl)-labeled AdML RNA oligonucleotides, which were pre-bound to full-length $U2AF^{65}$ (either with or without the $U2AF^{35}$ UHM subunit). The $SF1_{1–255}$ or phospho-$SF1_{1–255}$ proteins were titrated into protein-RNA complexes (*A*) Fl-$AdML_L$-$U2AF^{65}$, (*B*) Fl-$AdML_L$-$U2AF^{65}$-$U2AF^{35}$ UHM, (*C*) Fl-$AdML_S$-$U2AF^{65}$-$U2AF^{35}$ UHM. Schematic diagrams of the experiments, shown above the plots, provide the RNA sequences (branchpoint in bold). The plots show representative fits of the fluorescence anisotropy changes during titration. Bar graphs of the apparent equilibrium affinity (K_A) values are plotted on the right. The apparent equilibrium dissociation constants ($K_D = K_A^{-1}$) and the standard deviations of three technical replicates are given.

consistent with the previously noted importance of electrostatic interactions between charged residues of the ULM and UHM (37). The phosphorylation-induced increase in

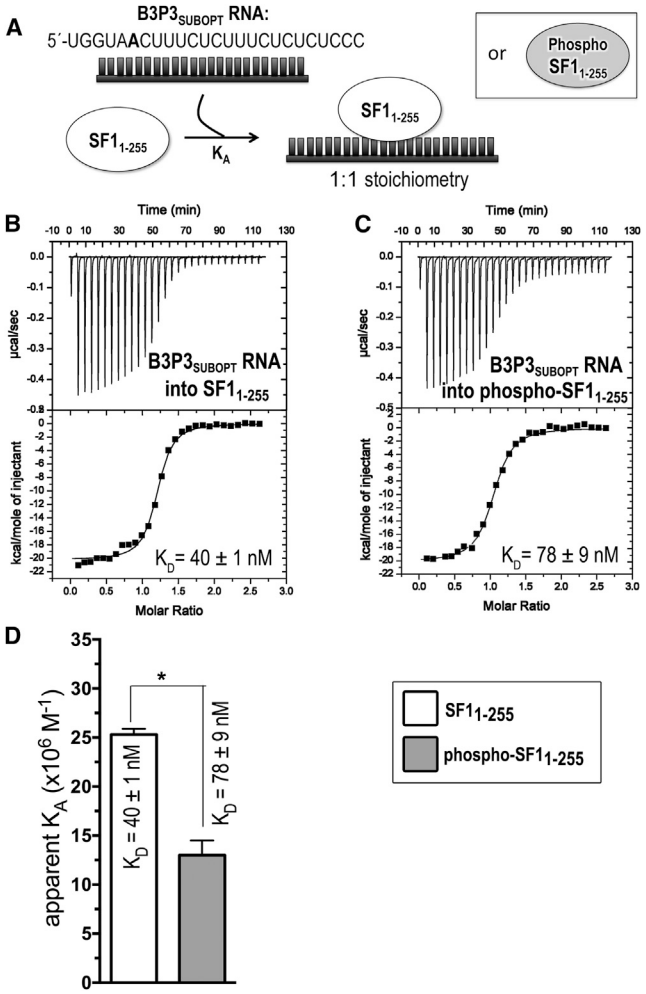

FIGURE 4 ITC results for $SF1_{1–255}$ (*white*) or phospho-$SF1_{1-255}$ (*gray*) titrated with B3P3 RNA. (*A*) Schematic diagram of the ITC experiment. (*B* and *C*) Representative isotherms fit with identical-site binding models. Titrations were of (*B*) 60 μM $B3P3_{SUBOPT}$ RNA into 5 μM $SF1_{1-255}$, c = 125; and (*C*) 60 μM $B3P3_{SUBOPT}$ RNA into 5 μM phospho-$SF1_{1–255}$, c = 64. Nonidentical-site models were discarded based on 1) little reduction in χ^2 for nonidentical sites compared to identical sites; 2) lower data/parameter ratio; and 3) fitting errors greater than the resulting values. (*D*) Bar graph of apparent affinities (K_A) of the interactions, colored as in (*A*). The apparent equilibrium dissociation constants ($K_D = K_A^{-1}$) and the standard deviations between at least two replicates are given.

SF1-$U2AF^{65}$ UHM affinity remained <2-fold, regardless of the higher salt concentration. Altogether, these data demonstrate that the free-energy change for SF1 binding to $U2AF^{65}$ after UHMK1 phosphorylation relative to unmodified SF1 ($\Delta\Delta G$) is less than expected for the gain of a single hydrogen-bond interaction. Nevertheless, the phosphorylation-induced enhancement of phospho-SF1-$U2AF^{65}$ association is reproducible and consistent with an ~2-fold greater retention of phosphorylated compared with unmodified SF1 by $U2AF^{65}$ in prior pull-down experiments (46).

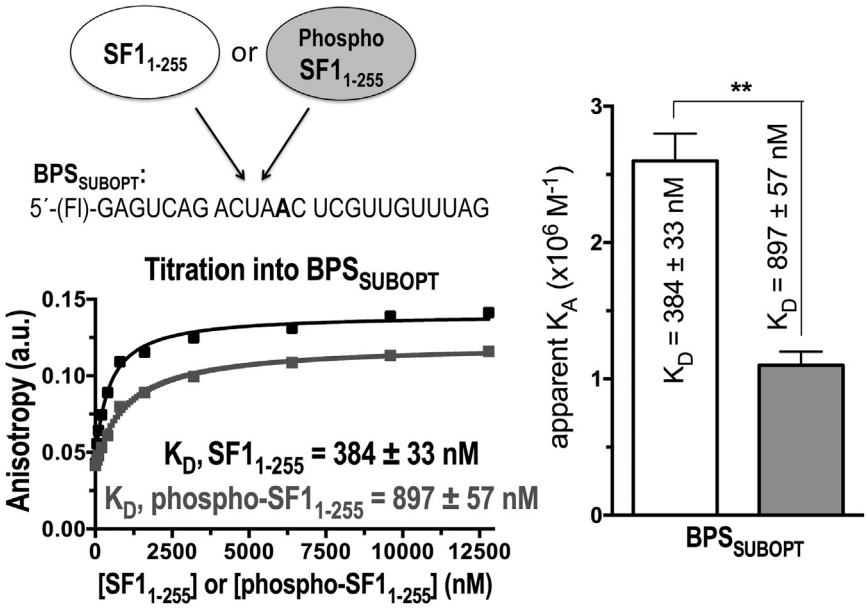

FIGURE 5 Fluorescence anisotropy RNA binding assays of $SF1_{1–255}$ or phospho-$SF1_{1–255}$ proteins titrated into BPS_{SUBOPT} RNA, represented as for Fig. 3.

UHMK1 phosphorylation slightly reduces SF1 affinities for off-target UHM proteins

Based on the steric prominence of the SF1 coiled-coil domain (42,43), we next hypothesized that phosphorylation-induced stabilization of this SF1 structure could reduce nonspecific binding to UHMs of other splicing factors. We focused on the UHMs of three splicing factors for which the cognate ULM partners are distinct from SF1: SPF45 and CAPERα, which are thought to recognize SF3b155 ULMs (40,41), and $U2AF^{35}$, which heterodimerizes with the $U2AF^{65}$ ULM (38). We found that phosphorylation by UHMK1 subtly penalized SF1 binding to these off-target UHMs (Fig. 2). The net specificity of SF1 for binding the $U2AF^{65}$ UHM improved from two- to sevenfold for the SPF45 UHM, from nearly 60- to 150-fold for the $U2AF^{35}$ UHM, and from 250-fold to >2300-fold for the CAPERα UHM (Fig. 2, *H* and *I*; Table 1). A fivefold reduced affinity of phospho-$SF1_{14-132}$ compared to the unmodified SF1 for binding the CAPERα UHM was the greatest change, whereas UHMK1-phosphorylation reduced SF1 binding to the UHMs of SPF45 or $U2AF^{35}$ by less than twofold. With the exception of the SPF45 UHM, SF1 phosphorylation consistently increased the magnitudes of both the enthalpy and entropy changes of UHM binding (Table 1). Considering a diminished effect in higher salt, the increase in the entropy-enthalpy compensation after phosphorylation of the $SF1_{14–132}$-$U2AF^{65}$ UHM complex may result from enhanced folding and/or coupled ion or proton exchange with the SPSP-containing loop, for which phosphate-arginine salt bridges mediate an ordered structure (42,43). Altogether, UHMK1-phosphorylation increased the net preference of phospho-SF1 slightly for binding to the $U2AF^{65}$ UHM relative to the SPF45 or $U2AF^{35}$ UHMs and showed a more substantial, sixfold net change in $U2AF^{65}$ versus CAPERα UHM specificity after SF1 phosphorylation.

UHMK1 phosphorylation slightly reduces SF1 affinity for AdML RNA in the presence of $U2AF^{65}$

Previously, others and we had shown that UHMK1 phosphorylation slightly enhances SF1 association with $U2AF^{65}$ by EMSA in the presence of sub-stoichiometric amounts of a radiolabeled RNA oligonucleotide (43,46). To further explore the influence of SPSP phosphorylation on the SF1 affinity for RNA in the presence of $U2AF^{65}$ in solution, we completed a variation of this experiment, in which we titrated increasing amounts of $SF1_{1–255}$ or phospho-$SF1_{1–255}$ into an equimolar mixture of $U2AF^{65}$ with 5′-fluorescein (Fl)-labeled RNA (Fig. 3).

We first tested the same protein constructs and RNA sequence as used in our prior EMSA, including phospho- or unmodified $SF1_{1–255}$, full-length $U2AF^{65}$, and a 34mer RNA corresponding to the prototypical 3′ splice site of adenovirus major late promoter transcript ($AdML_L$) (Fig. 3 *A*). To our surprise, phosphorylation by UHMK1 slightly decreased (by threefold) rather than enhanced SF1 binding to the $AdML_L$ RNA in the presence of $U2AF^{65}$. To rule out whether the apparent phosphorylation-induced decrease in affinity was affected by aggregation of full-length $U2AF^{65}$, we repeated the experiment after co-purification of $U2AF^{65}$ with the $U2AF^{35}$ UHM (Fig. 3 *B*), which improves the solubility and monodispersity of the U2AF protein preparation. Phosphorylation again decreased rather than enhanced SF1 binding to the $AdML_L$ RNA in the presence of the $U2AF^{65}$-$U2AF^{35}$ UHM complex by the same amount (threefold) as for $AdML_L$ RNA in the presence of

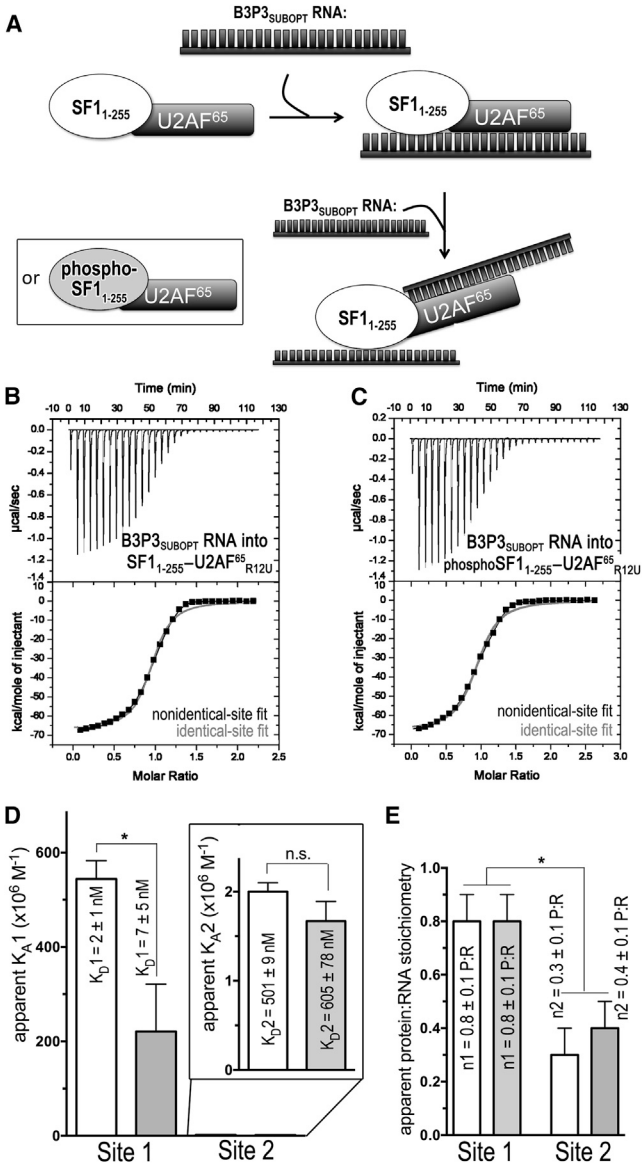

FIGURE 6 ITC results for $SF1_{1–255}$-$U2AF^{65}{}_{R12U}$ (*white*) or phospho-$SF1_{1–255}$-$U2AF^{65}{}_{R12U}$ (*gray*) protein complexes titrated with $B3P3_{SUBOPT}$ RNA. (*A*) Schematic diagram of the ITC experiment. (*B* and *C*) Representative isotherms fit with binding models for either nonidentical sites (*black lines*) or identical sites (*red lines*). Titrations were of (*B*) 35 μM B3P3 RNA into 5 μM $SF1_{1–255}$-$U2AF^{65}{}_{R12U}$ complex (nonidentical sites, χ^2 = 0.20E6 ± 0.16E6; identical sites, χ^2 = 2.70E6 ± 0.29E6), c = 5000 for site 1 and c = 10 for site 2; and (*C*) 35 μM B3P3 RNA into 5 μM phospho-$SF1_{1–255}$-$U2AF^{65}{}_{R12U}$ complex (nonidentical sites, χ^2 = 0.23E6 ± 0.19E6; identical sites, χ^2 = 3.13E6 ± 0.95E6), c = 700 for site 1 and c = 8 for site 2. The identical site models were discarded based on the large χ^2 increase, poor fit, and nonidentical sites of reverse titrations (Fig. S5). (*D*) Bar graph of apparent affinities (K_A) of the interactions, colored as for (*A*). The apparent equilibrium dissociation constants ($K_D = K_A^{-1}$) and the standard deviations of at least two replicates are given. An expanded view of the lower affinity sites is inset. (*E*) Bar graph of apparent protein:RNA stoichiometries (n).

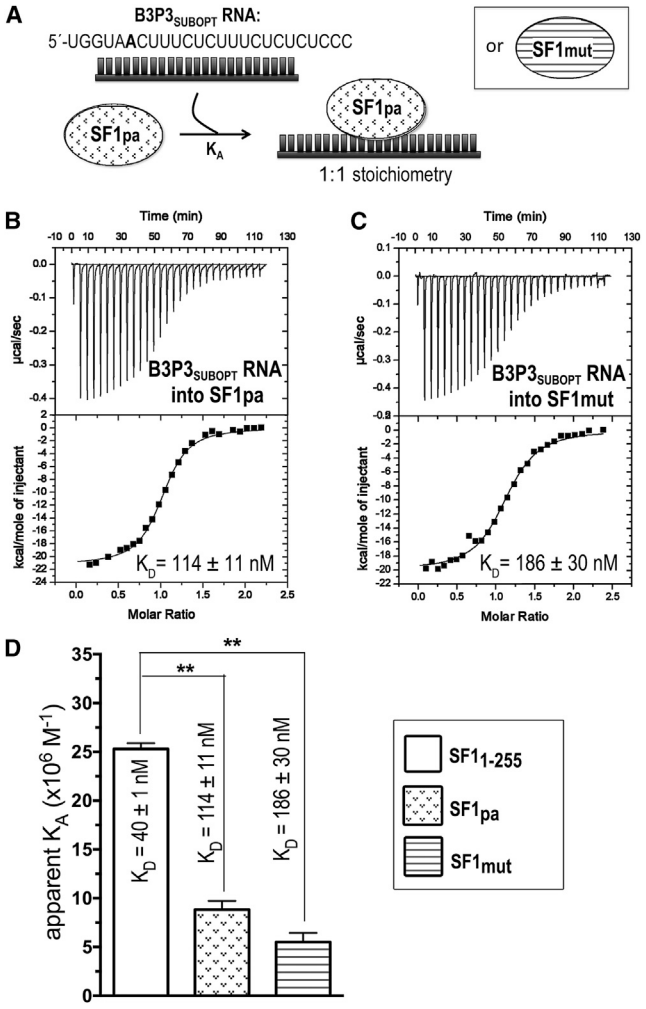

FIGURE 7 ITC results for SF1mut (*striped*) or SF1pa (*stippled*) titrated with B3P3 RNA. (*A*) Schematic diagram of the ITC experiment. (*B* and *C*) Representative isotherms fit with identical-site binding models for (*B*) 50 μM $B3P3_{SUBOPT}$ RNA into 5 μM SF1pa, c = 44, and (*C*) 50 μM $B3P3_{SUBOPT}$ RNA into 5 μM SF1mut, c = 27. (*D*) Bar graph of apparent affinities (K_A) of the interactions, colored as in (*A*). The K_A of unmodified $SF1_{1–255}$ (*white*) is plotted for comparison. The inset shows apparent equilibrium dissociation constants ($K_D = K_A^{-1}$) and standard deviations of at least two replicates.

$U2AF^{65}$. To avoid possible alternative binding sites due to inclusion of sequences flanking the splice site, which none of the SF1, $U2AF^{65}$, or $U2AF^{35}$ UHM subunits are expected to recognize, we compared titrations of SF1 or phospho-SF1 into a stoichiometric mixture of $U2AF^{65}$-$U2AF^{35}$ UHM incubated with a 25mer 5′-Fl-RNA comprising the core BPS and Py tract of the AdML 3′ splice site ($AdML_S$) (Fig. 3 *C*). The affinities of unmodified SF1 for $AdML_L$ and $AdML_S$ in the presence of $U2AF^{65}$-$U2AF^{35}$-UHM were indistinguishable. The phosphorylation-induced decrease in protein-RNA affinity was slightly greater for the $AdML_S$ RNA, possibly due to limited binding registers on the minimal sequence. The nearly sevenfold decrease in binding affinity of phosphorylated compared to unmodified SF1 for $AdML_S$ in the presence of $U2AF^{65}$-$U2AF^{35}$ UHM corresponds to a $\Delta\Delta G$ that is similar in magnitude to the loss of a strong hydrogen bond.

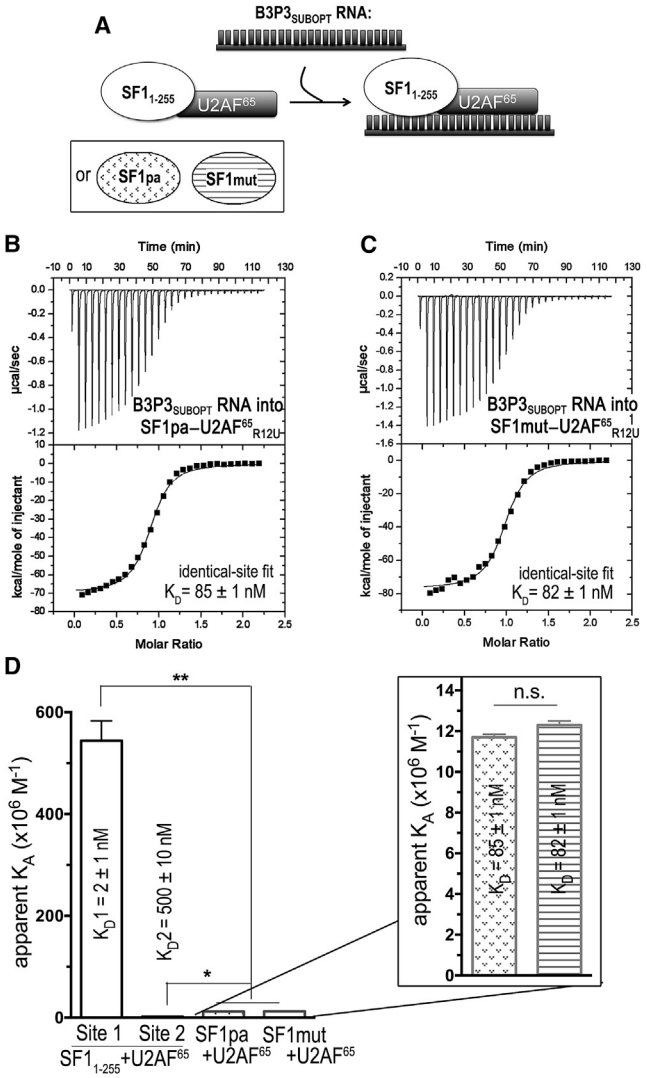

FIGURE 8 ITC results for SF1mut-U2AF$^{65}{}_{R12U}$ (*striped*) or SF1pa-U2AF$^{65}{}_{R12U}$ (*stippled*) complexes titrated with B3P3$_{SUBOPT}$ RNA. (*A*) Schematic diagram of the ITC experiment. (*B* and *C*) Representative isotherms fit with identical site models for (*B*) 50 μM B3P3 RNA into 5 μM SF1pa-U2AF$^{65}{}_{R12U}$ complex, c = 59, and (*C*) 50 μM B3P3 RNA into 5 μM SF1mut-U2AF$^{65}{}_{R12U}$ complex, c = 61. Nonidentical-site models were discarded based on 1) fitting errors greater than the resulting thermodynamic values; 2) stoichiometry values of nearly zero for one class of nonidentical sites; and 3) thermodynamic values for the remaining class of sites that matched the results of the identical-site fit. (*D*) Bar graph of apparent affinities (K_A) of the interactions, colored as in (*A*). The apparent equilibrium dissociation constants ($K_D = K_A^{-1}$) and standard deviations of at least two replicates are given. For comparison, the nonidentical-site affinities of the parent SF1$_{1–255}$-U2AF$^{65}{}_{R12U}$ complex titrated with B3P3 RNA (details in Fig. 6) are plotted at left. The inset shows an expanded view of the B3P3 RNA affinities for the SF1mut- or SF1pa-U2AF$^{65}{}_{R12U}$ complexes. A control titration of B3P3$_{SUBOPT}$ RNA into buffer is shown in Fig. S1 *C* and a titration of B3P3$_{SUBOPT}$ RNA into SF1mut-U2AF$^{65}{}_{R12U}$ in phosphate buffer (as opposed to HEPES) is shown in Fig. S6.

A posteriori, we realized that in prior EMSA experiments, association of SF1 with U2AF^{65} dominated the apparent binding constants due to a large excess of U2AF^{65} compared to the radiolabeled RNA (>50-fold), coupled with the significantly higher RNA affinity of the SF1-U2AF^{65} complex compared to either subunit alone (55). As such, the increase in shifted RNA in the EMSA recapitulated the phosphorylation-induced increase in the affinity of SF1 for binding U2AF^{65}, described above. In the titrations of SF1 into stoichiometric mixtures of fluorescently labeled RNA and U2AF^{65} here, approximately half of the U2AF^{65} and RNA molecules are dissociated in the sample cell before titration with SF1 (estimated from the ~30 nM K_D of the full-length U2AF^{65}-U2AF^{35} UHM complex binding the AdML Py tract (56) and a 25 nM concentration of U2AF^{65}-U2AF^{35} UHM protein and RNA in the sample cell). Considering the many competing equilibria (Fig. S3), only apparent binding constants for the experiments are given in Fig. 3. Regardless, we observed a consistent reduction in the apparent RNA affinity of phosphorylated compared to unmodified SF1 in all three U2AF^{65}-containing RNA mixtures (U2AF^{65}-AdML$_L$, U2AF^{65}-U2AF^{35} UHM-AdML$_L$, U2AF^{65}-U2AF^{35} UHM-AdML$_S$), which we then proceeded to test in better-defined systems.

UHMK1-phosphorylation slightly reduces SF1 affinity for splice-site RNAs

The decreased affinity of phospho-SF1 relative to unmodified SF1 for U2AF^{65}-containing–RNA complexes, yet slightly enhanced phospho-SF1 binding to apo-U2AF^{65}, implied that RNA binding by SF1 or SF1-U2AF^{65} was inhibited by UHMK1 phosphorylation. To test this possibility in a defined system, we measured the affinities of phosphorylated versus unmodified SF1 binding an RNA splice site by ITC (Fig. 4; Table 2), a quantitative method that fits the enthalpy changes of binding to obtain the apparent equilibrium dissociation constant (K_D). In our prior EMSAs (42), phosphorylated versus unmodified SF1 bound with similar apparent affinities to the AdML$_L$ RNA, which is a "strong," near-consensus splice site. Yet in other hands, EMSAs suggested that SRPK2 phosphorylation of S82 slightly enhances SF1 binding to "weak" splice sites that poorly match the BPS consensus (47). With these considerations, we tested SF1 binding to a variant of a well-characterized "B3P3" splice site from α-tropomyosin (B3P3$_{SUBOPT}$) (57), for which a -3/-4GG sequence preceding the branch-point is expected to decrease SF1 affinity by approximately threefold (58). Phosphorylation of SF1$_{1–255}$ by UHMK1 decreased affinity for the B3P3$_{SUBOPT}$ RNA by twofold. This free-energy change ($\Delta\Delta G$) of a ~0.5 kcal mol^{-1} resulted from a 2.5 kcal mol^{-1} penalty for the enthalpy change ($\Delta\Delta H$) and −2 kcal mol^{-1} favorable contribution to the entropy change [$\Delta(-T\Delta S)$]. These thermodynamic differences agree with ordering of the SPSP-loop conformation after phosphorylation, and they further allude to the possibility of enthalpically favorable contacts between

this region in the unphosphorylated state and the bound RNA site.

Although we weakened the BPS of our $B3P3_{SUBOPT}$ splice site, it remained possible that phosphorylation-enhanced RNA binding affinity would manifest only in the context of extreme suboptimal BPS such as that tested in EMSAs after SRPK2-phosphorylation of SF1 (47). To evaluate this possibility, we compared the affinities of UHMK1-phosphorylated and unmodified SF1 for binding an identical RNA oligonucleotide (BPS_{SUBOPT}) as the prior, SRPK2-focused EMSA study. We used the fluorescence anisotropy RNA binding assay to determine the K_D, since the affinities of RNA binding were relatively low for reliable measurement by ITC. The affinity of SF1 for the BPS_{SUBOPT} oligonucleotide decreased more than twofold after UHMK1 phosphorylation, similar to the change we observed by ITC with the $B3P3_{SUBOPT}$ splice site (Fig. 5). The subtle, yet consistent, decrease in the affinity of phospho-SF1 relative to unmodified SF1 for splice-site RNA explained the reduced phospho-SF1 affinity for the pre-formed $U2AF^{65}$-RNA complex that we had observed by fluorescence anisotropy assays.

UHMK1 phosphorylation slightly reduces SF1-$U2AF^{65}$ affinity for a splice-site RNA

We next asked whether UHMK1 phosphorylation would affect RNA binding by the relevant, SF1-$U2AF^{65}$ complex. To address this question, we used ITC to compare UHMK1-phosphorylated to unmodified $SF1_{1–255}$-$U2AF^{65}{}_{R12U}$ complexes binding the $B3P3_{SUBOPT}$ RNA (Fig. 6; Table 3). First, we titrated the $B3P3_{SUBOPT}$ RNA into the unmodified or phospho-$SF1_{1–255}$-$U2AF^{65}{}_{R12U}$ protein complex, which had been prepared by size-exclusion chromatography from a stoichiometric mixture of the pre-purified subunits. By placing the proteins in the sample cell ([$SF1_{1–255}$-$U2AF^{65}{}_{R12U}$] = 5000 nM), we avoided potential heats of dilution due to complex dissociation, which nevertheless were unlikely considering the high affinity of the SF1-$U2AF^{65}$ complex (60 nM; Table 1). The isotherms were best fit by nonidentical-site models considering both visual inspection and reduction in χ^2 (Fig. 6, *B* and *C*). The apparent stoichiometries of the two classes of sites (Fig. 6 *E*) suggested that SF1 (or phospho-SF1) and $U2AF^{65}$ each bound separate RNA oligonucleotides in the presence of excess RNA (Fig. 6 *A*). Indeed, the $B3P3_{SUBOPT}$ RNA affinity of the second site agrees with the affinity of the isolated $U2AF^{65}$ subunit (K_D = 500 nM and 509 nM; Fig. S4), suggesting that a second RNA molecule replaces $U2AF^{65}$ contacts with the intramolecular Py tract of $B3P3_{SUBOPT}$ bound to the $SF1_{1–255}$-$U2AF^{65}{}_{R12U}$ complex (Fig. 6 *A*). Regardless of the model chosen for the fit (identical versus nonidentical sites), a similar subtle penalty for RNA binding was observed after SPSP-phosphorylation of SF1.

To confirm the nonidentical-binding-site model, we next reversed the ITC experiment and titrated the $SF1_{1–255}$-$U2AF^{65}{}_{R12U}$ complex into $B3P3_{SUBOPT}$ RNA (Fig. S5). A control titration of $SF1_{1–255}$-$U2AF^{65}{}_{R12U}$ into buffer was linear and showed negligible heats of dilution (Fig. S1 *D*). We expected that the isotherms of the reverse titrations would best fit nonidentical-binding-site models and that a low-affinity binding site with an apparent stoichiometry of two RNA molecules per protein complex would be evident during the early (as opposed to late) steps of the titration, for which the RNA is in molar excess over protein molecules. Accordingly, the isotherms were best fit by nonidentical-site binding models by visual inspection and reduction in χ^2 (Fig. S5, *B* and *C*). The apparent stoichiometries of the two classes of binding sites (Fig. S5 *E*) agreed with initial binding of two RNA oligonucleotides per one $SF1_{1–255}$-$U2AF^{65}{}_{R12U}$ (or phospho-$SF1_{1–255}$-$U2AF^{65}{}_{R12U}$) complex, presumably one RNA per SF1 or $U2AF^{65}$ subunit (Fig. S5 *A*), when RNA is in large excess over protein during the early stage of this reverse titration. The higher-affinity class of binding sites with 1:1 stoichiometry of $SF1_{1–255}$-$U2AF^{65}{}_{R12U}$ (or phospho-$SF1_{1–255}$-$U2AF^{65}{}_{R12U}$) per RNA oligonucleotide, becomes apparent in the later stages of titration as protein concentrations rise relative to RNA. The higher-affinity binding site of the reverse titration includes an unfavorable contribution from the dissociation of one RNA molecule from the 2:1 complex before rebinding to form the $SF1_{1–255}$-$U2AF^{65}{}_{R12U}$-RNA (or phospho-$SF1_{1–255}$-$U2AF^{65}{}_{R12U}$-RNA) complex with 1:1 stoichiometry. As such, we focus on interpreting the high-affinity binding site of the $B3P3_{SUBOPT}$ RNA titration into $SF1_{1–255}$-$U2AF^{65}{}_{R12U}$ (or phospho-$SF1_{1–255}$-$U2AF^{65}{}_{R12U}$) complexes. Phosphorylation by UHMK1 consistently reduced the apparent $B3P3_{SUBOPT}$ RNA affinity of the SF1-$U2AF^{65}$ complex by ~3-fold for the high-affinity sites of either the forward or reverse titrations (Table 3), which is similar to the penalty observed for the isolated SF1 subunit.

SF1 coiled-coil domain contributes to SF1 or SF1-$U2AF^{65}$ binding a splice-site RNA

The slight energetic, yet more significant enthalpic, penalties for RNA binding after phosphorylation of SF1 ($\Delta\Delta G$ = 0.5 kcal mol^{-1} and $\Delta\Delta H$ = 3 kcal mol^{-1}) left open the possibility that the SF1 coiled coil might contact RNA. To explore this possibility, we first swapped the SF1 coiled coil for an unrelated three-helix bundle from *Staphylococcus aureus* protein A to generate a chimeric "SF1pa" protein (Fig. 1 *B*). We flanked the protein-A domain with 25-amino-acid glycine-rich linkers with the intention of structurally uncoupling the protein A region from the surrounding UHM-bound SF1 ULM and KH-QUA2 RNA binding domain. The total number of amino acids remained unchanged between the $SF1_{1–155}$ parent and SF1pa chimera. Likewise, the isoelectric points (pI), and hence net charges, of the phosphorylated SF1 coiled coil and the artificial protein-A domain were similar (pI = 5.1 and 5.5 compared with

6.8 for the unmodified coiled-coil domain). The substituted domain reduced the apparent affinity of the SF1pa protein for the $B3P3_{SUBOPT}$ RNA by ~3-fold compared to unmodified $SF1_{1–255}$ (Fig. 7). This penalty for RNA binding, as well as the underlying enthalpy and entropy changes, were nearly indistinguishable between SF1pa and phospho-$SF1_{1–255}$ (Table 3), which suggested that the protein-A chimera had an effect on SF1-RNA binding similar to that observed for SPSP phosphorylation, at least in the context of the isolated SF1 subunit.

We next extended our investigation of the SF1 coiled coil to the consequences of its protein A substitution for RNA binding in the context of the SF1-$U2AF^{65}$ complex. We monitored, by ITC, SF1pa-$U2AF^{65}{}_{R12U}$ binding the $B3P3_{SUBOPT}$ RNA (Fig. 8). In contrast to the isotherms of wild-type SF1-$U2AF^{65}$ complexes binding RNA, an identical-site binding model with an apparent 1:1 stoichiometry adequately fit the SF1pa-$U2AF^{65}{}_{R12U}$ isotherms (Fig. 8, *B* and *C*). The apparent loss of the nonidentical RNA binding site suggested that steric hindrance or other effects prevented binding of two separate RNAs to the SF1pa-$U2AF^{65}{}_{R12U}$ heterodimer at the concentrations used in our ITC experiment. Notably, the SF1pa-$U2AF^{65}{}_{R12U}$ affinity for the $B3P3_{SUBOPT}$ RNA decreased by ~40-fold relative to the high-affinity SF1-$U2AF^{65}{}_{R12U}$-$B3P3_{SUBOPT}$ RNA site (Fig. 8 *D*). This large penalty of the SF1 domain substitution for RNA binding by the SF1pa-$U2AF^{65}{}_{R12U}$ complex significantly exceeded its threefold impact on RNA binding by the SF1 subunit, and also exceeded the threefold penalty incurred by UHMK1 phosphorylation of the protein complex. We conclude that the SF1 coiled-coil domain is required for high-affinity association of the SF1-$U2AF^{65}$ complex with a representative $B3P3_{SUBOPT}$ splice site.

Arginines at the phosphorylation site contribute to SF1 or SF1-$U2AF^{65}$ binding a splice-site RNA

We next tested a potential role in RNA binding for key arginine residues in the SPSP-containing SF1 loop (R93, R97, and R100), which otherwise coordinate the phosphorylated serines in a structured conformation for the phosphorylated state (42,43) (Fig. 1 *C*). We previously had found that SF1 carrying glutamate mutations of these three arginines (R93E/R97E/R100E) was unable to restore cell proliferation after SF1 knockdown (42). We first used ITC to determine the thermodynamic consequences of the R93E/R97E/R100E mutations in the $SF1_{1–255}$ construct (SF1mut; Fig. 1 *B*) for binding the representative $B3P3_{SUBOPT}$ splice-site RNA. The arginine mutations penalized the RNA binding affinity of SF1mut by nearly fivefold relative to wild-type $SF1_{1–255}$ (Fig. 7). The enthalpy and entropy changes underlying $B3P3_{SUBOPT}$ RNA binding by the isolated SF1mut subunit resembled those of phospho-$SF1_{1–255}$ and SF1pa more than the unmodified SF1 (Table 2). An enthalpic penalty, $\Delta\Delta H$, after introduction of the glutamates (3.3 kcal mol^{-1}) overcame a lesser $\Delta(-T\Delta S)$ (−2.3 kcal mol^{-1}) for the mutant compared to wild-type $SF1_{1–255}$ subunits. The slight $\Delta\Delta G$ of 1 kcal mol^{-1} between SF1mut and $SF1_{1–255}$ would agree with disruption of a single hydrogen bond rather than three ion pairs. On the other hand, the compensation of a large unfavorable entropy change by a larger enthalpy change for SF1mut-RNA binding would agree with structuring of the unphosphorylated, arginine-containing loop for RNA interactions.

We next tested the influence of the SF1 arginine mutations on $B3P3_{SUBOPT}$ RNA recognition in the context of the SF1mut-$U2AF^{65}{}_{R12U}$ complex. The $B3P3_{SUBOPT}$ RNA affinity of SF1mut-$U2AF^{65}{}_{R12U}$ was indistinguishable from that of SF1pa-$U2AF^{65}{}_{R12U}$ (Table 3). In both cases, identical-binding-site models adequately fit the isotherms (Fig. 8, *B* and *C*). Also, as for SF1pa-$U2AF^{65}{}_{R12U}$, the $B3P3_{SUBOPT}$ RNA binding affinities of SF1mut-$U2AF^{65}{}_{R12U}$ decreased by 40-fold relative to the high-affinity, stoichiometric site of unmodified SF1-$U2AF^{65}{}_{R12U}$ (Fig. 8 *D*).

The enthalpy and entropy changes of all variant SF1-$U2AF^{65}{}_{R12U}$ complexes binding the $B3P3_{SUBOPT}$ RNA (including those of the unmodified $SF1_{1–255}$, phospho-SF1, SF1pa, and SF1mut complexes with $U2AF^{65}$) are remarkably large in magnitude (Table 3). In general, these thermodynamic changes are likely to be dominated by RNA association with the $U2AF^{65}$ RRMs. In our previous ITC experiments that contained BES buffer, we had shown large enthalpy and entropy changes underpinning cognate RNA binding by tandem RRMs, including those of $U2AF^{65}{}_{R12U}$, Sex-Lethal, and poly-A binding protein (59). For comparison with other ITC experiments herein, we here recapitulated this result for $B3P3_{SUBOPT}$ RNA binding by $U2AF^{65}{}_{R12U}$ in a HEPES-containing buffer (Fig. S4; Table 2).

Even so, the magnitudes of the enthalpy and entropy changes for $B3P3_{SUBOPT}$ RNA binding were notably greater for the SF1mut-$U2AF^{65}{}_{R12U}$ compared to the unmodified $SF1_{1–255}$-$U2AF^{65}{}_{R12U}$ complexes ($\Delta\Delta H$ of −16.6 kcal mol^{-1} and $\Delta(-T\Delta S)$ of 19 kcal mol^{-1}). In comparison, these thermodynamic changes of RNA binding were similar between the phospho-$SF1_{1–255}$-$U2AF^{65}{}_{R12U}$ and the unmodified complex ($\Delta\Delta H$ and $\Delta(-T\Delta S)$ were −0.3 kcal mol^{-1} and 1 kcal mol^{-1}). Although the enthalpy and entropy changes of SF1pa-$U2AF^{65}{}_{R12U}$ binding the $B3P3_{SUBOPT}$ RNA were slightly greater in magnitude than those of the $SF1_{1–255}$-$U2AF^{65}{}_{R12U}$ complex ($\Delta\Delta H$ and $\Delta(-T\Delta S)$ were −7.4 kcal mol^{-1} and 9.8 kcal mol^{-1}), they also were significantly less than those of SF1mut-$U2AF^{65}{}_{R12U}$.

One possible explanation for the larger magnitudes of the enthalpy and entropy changes for the SF1mut-$U2AF^{65}{}_{R12U}$ complex binding RNA is that mutations of the ionizable arginine residues alter proton exchange between the RNA-bound complex and its surroundings. In an effort to avoid potential interactions between a phosphate buffer and

allosteric or RNA binding sites of the proteins, we had used a HEPES buffer, which has a relatively large enthalpy of ionization (5 kcal mol^{-1} (60)). We repeated the experiment with the SF1mut-U2AF$^{65}_{R12U}$ complex titrated with B3P3$_{SUBOPT}$ RNA in sodium phosphate buffer (Fig. S6), which has a relatively low ionization enthalpy (1 kcal mol^{-1} (60)). The magnitudes of the enthalpy and entropy changes for the mutant complex binding RNA in the phosphate buffer decreased to nearly match the values for the protein-A domain-substituted complex in HEPES buffer ($\Delta\Delta H$ of -0.9 kcal mol^{-1} and $\Delta(-T\Delta S)$ of 0.9 kcal mol^{-1} between RNA titrations of SF1pa-U2AF$^{65}_{R12U}$ or SF1mut-U2AF$^{65}_{R12U}$ complexes in respective phosphate or HEPES buffers) (Table 3). The buffer-dependent alteration in the enthalpy change was consistent with loss of approximately three additional protons from the mutant compared to the wild-type protein (site 1) on formation of the RNA complex, consistent with changed acid dissociation constants of three ionizable residues by the three arginine-to-glutamate mutations.

Altogether, these ITC experiments demonstrate that both the coiled-coil region of SF1 and the arginine residues surrounding the phosphorylation site are important for recognition of a representative splice site by the SF1-U2AF^{65} complex.

DISCUSSION

Phosphorylation is an emerging means for regulating UHM-ULM interactions. Here, we show that phosphorylation of tandem serines in a conserved SPSP motif of SF1 enhances specific association with its U2AF^{65} partner and inhibits binding to representative splice-site RNAs. The effect of phosphorylation on the UHM-binding specificity of SF1 is subtle. Considering both the enhanced binding of phosphorylated SF1 to U2AF^{65} and its diminished association with other UHMs, the net increase in the binding specificity of U2AF^{65} for phosphorylated relative to unphosphorylated SF1 is typically three- to fourfold. The binding affinities of SF1 for the U2AF^{35} or CAPERα UHMs are significantly lower than for U2AF^{65}, whereas the SF1 affinity for SPF45 approaches its affinity for U2AF^{65} (by ~2-fold). As such, SPSP phosphorylation appears most relevant for avoiding unintended SF1 complexes with SPF45, although other UHMs also could compete for binding the SF1 ULM depending on their local relative abundance.

In a prior EMSA study, phosphorylation of SF1 by SRPK2, which selectively phosphorylates S82 of the SPSP motif as opposed to both S80 and S82, appeared to slightly enhance rather than inhibit SF1 binding to splice-site RNAs containing suboptimal BPSs (47). In contrast, our quantitative fluorescence anisotropy RNA binding assays here demonstrate that phosphorylation of both S80 and S82 by UHMK1 reduces SF1 affinity for a BPS$_{SUBOPT}$ RNA oligonucleotide that shares the same sequence as the major oligonucleotide of the prior study as well as a distinct B3P3-splice-site RNA. Several key differences distinguish our experiments from the prior study. A major distinction is that SRPK2 predominately phosphorylates S82 of human SF1 (47), whereas UHMK1 phosphorylates both serines of the SPSP motif (42,46). The SPSP motif of SF1 is predominately found in the phosphorylated state in proliferating cells (46), and the majority of SF1 remains phosphorylated after knockout of UHMK1 in mice (48). As such, the SF1 SPSP motif is likely to be regulated by a multitude of different kinases and phosphatases, including, but not limited to, UHMK1 (46), SPRK2 (47), and possibly hPrp4 (61), for a potentially broad variety of distinct functions. Several technical differences also distinguish experiments in the prior study (47) from our experiments here, including the presence of SRPK2 and ATP in the prior binding experiment (rather than purified phospho-SF1 used in our procedures here), use of the isolated SF1 subunit rather than the SF1-U2AF^{65} complex, different migration of phosphorylated versus unmodified proteins (62), and the non-equilibrium nature of EMSAs, which may be affected by separation of the RNA ligand from the protein partner during the course of electrophoresis.

Thermodynamic changes are challenging to interpret in terms of protein structure, due to the multiple processes linked to the binding event that are simultaneously detected in an ITC experiment. Nonetheless, potential insights may be gleaned by examining the apparent enthalpy and entropy changes of the binding experiments, which are strengthened by comparisons among the variant complexes. The remarkably large magnitudes of the enthalpy and entropy changes for B3P3$_{SUBOPT}$ RNA binding by the SF1-U2AF^{65} complex (unmodified or phosphorylated) are likely to result from RNA binding by the U2AF^{65} RRMs, which have characteristically large enthalpy and entropy changes (59). Perhaps coincidentally, the enthalpy and entropy changes for the chimeric SF1pa-U2AF^{65} complex binding the B3P3$_{SUBOPT}$ RNA resemble those of the second RNA binding site of the unmodified SF1-U2AF^{65} complex, which appears to represent the different subunits of the complex each binding separate RNAs at high RNA/SF1-U2AF^{65} molar ratios. This thermodynamic similarity could reflect analogous uncoupling of the SF1 and U2AF^{65} RNA binding domains by the artificial protein-A replacement of the natural coiled coil.

Consistent with the protein-A domain replacement uncoupling the SF1 and U2AF^{65} RNA binding domains, cooperative RNA binding by the SF1-U2AF^{65} complex (as defined by increased RNA binding by the protein complex relative to the individual proteins) is lost in the SF1pa-U2AF^{65} complex. Specifically, the SF1-U2AF^{65} affinity for the B3P3$_{SUBOPT}$ RNA is nearly 20-fold greater than the summed affinities of the individual subunits (50E7 M^{-1} compared to 2.7E7 M^{-1}), whereas the SF1pa-U2AF^{65} affinity for binding the B3P3$_{SUBOPT}$ RNA is indistinguishable from the summed

RNA affinities of the separate subunits (1.2E7 M^{-1} compared to 1.1E7 M^{-1}). Remarkably, mutation of the arginines at the phosphorylation site to glutamates results in a similar loss of cooperative RNA binding by the SF1mut-$U2AF^{65}$ complex (1.2E7 M^{-1} compared to 0.74E7 M^{-1}). Although the substituted domain from protein A is a three-helix bundle rather than a two-helix coiled coil, relatively long (25-residue) glycine-rich linkers were included to permit flexible orientations among the connected domains. Accordingly, the RNA/SF1pa-$U2AF^{65}$ stoichiometry (as well as the RNA/SF1mut-$U2AF^{65}$ complex) remains 1:1, supporting the capacity of both subunits to bind the same RNA in these mutated complexes. Although SPSP phosphorylation slightly decreases inter-subunit cooperativity ($B3P3_{SUBOPT}$ RNA affinity of phospho-SF1-$U2AF^{65}$ is 14.3E7 M^{-1}, compared to 1.5E7 M^{-1} from the summed RNA affinities of phospho-SF1 and $U2AF^{65}$), the effect remains relatively subtle (a twofold decrease compared to the unphosphorylated complex). Altogether, these observations suggest that the SF1 coiled-coil domain and arginine-containing SPSP loop actively couple the SF1 and $U2AF^{65}$ subunits for synergistic recognition of the 3′-splice-site RNA.

The reduced binding affinity of the phospho-SF1-$U2AF^{65}$ complex for the negatively charged RNA is chemically intuitive, considering that two negatively charged phosphates are introduced in the UHMK1-phosphorylated SPSP motif. The large reduction in the apparent $B3P3_{SUBOPT}$ RNA affinity of SF1mut-$U2AF^{65}$ relative to the wild-type SF1-$U2AF^{65}$ complexes (50E7 M^{-1} compared to 1.2E7 M^{-1}) further suggests that the mutated arginines, which otherwise coordinate the phosphorylated SPSP motif, could interact with RNA in the unmodified state. Given the many possible phosphorylation-dependent processes linked to the RNA binding event, such as global domain orientation and local conformation of the SPSP-containing loop, whether phosphorylation directly interferes with RNA contacts remains an open question. Direct RNA contacts by the arginine-rich SF1 loop in which the SPSP motif resides would reconcile a disparity between natural BPS-Py tract spacings and piecewise SF1-BPS and $U2AF^{65}$-Py tract structures. The branched intron lariat preferentially forms over a range of ~18–40 nucleotides from the 3′-splice-site junction (63,64), and the branchpoint adenosine typically is separated from the start of the Py tract by eight poorly conserved nucleotides (64). Yet the known RNA interactions of the structurally characterized SF1 and $U2AF^{65}$ domains encompass only three nucleotides after the branchpoint adenosine (65,66) and nine pyrimidine nucleotides (56,67), leaving approximately five intervening nucleotides unaccounted for. Based on available structures, the SF1 coiled coil could act as an inert ruler of the BPS-Py tract spacing. In light of the data presented here, we further propose that this SF1 region plays an active role in synergistic positioning of the SF1 and $U2AF^{65}$ domains for RNA binding. It is possible that phosphorylation of the SF1 SPSP motif by UHMK1 reduces SF1-$U2AF^{65}$-RNA recognition by diverting these key arginine residues for interactions with the phosphorylated serines as opposed to RNA.

Future experiments are needed to fully resolve the mechanisms underpinning the importance of SPSP phosphorylation for cell proliferation (42). At face value, the observations that SF1 phosphorylation promotes specific binding to its $U2AF^{65}$ partner, yet reduces binding of the SF1-$U2AF^{65}$ complex to 3′ splice sites, seem incongruous. One possible explanation is that the phosphorylation of the SF1 SPSP motif before pre-mRNA splicing might both facilitate specific assembly of the phospho-SF1-$U2AF^{65}$ complex and also inhibit premature association of this complex with RNAs. Co-transcriptional dephosphorylation could then promote loading of SF1-$U2AF^{65}$ on the emerging pre-mRNA during the early stages of splicing. Accordingly, SF1 associates with $U2AF^{65}$ in extra-spliceosomal complexes (6), and phosphorylation and dephosphorylation events such as this one are required for pre-mRNA splicing (e.g., (68–70)). Indeed, the influences of SPSP phosphorylation on any SF1 functions other than UHM and RNA interactions have yet to be examined. The lack of SF1-dependent in vitro splicing substrates rules out biochemical reconstitution assays of pre-mRNA splicing activity. Whether SPSP phosphorylation could regulate SF1 roles in nuclear pre-mRNA retention (2) and transcriptional repression (32,33) also remains unknown. It further remains possible that SPSP phosphorylation may promote relocalization of SF1 in the cell; the SRPK2 kinase that can phosphorylate S82 in the SPSP motif of human SF1 is known to redistribute the nuclear localization of other splicing factors (71). A precedent for phosphorylation-dependent ULM-protein interactions has been set for the case of ATX1 (45,72). Phosphorylation of S776 adjacent to the ATX1 ULM slightly reduces its affinity for the $U2AF^{65}$ or SPF45 UHM (45), comparable to the reduced binding of phospho-SF1 to the SPF45, $U2AF^{35}$, or CAPERα UHM noted here. Conversely, ATX1 phosphorylation promotes its association with the 14-3-3 signaling protein. By analogy with the ATX1 precedent, a subtle influence of SPSP phosphorylation on SF1-UHM interactions could accompany a more drastic impact on SF1 binding to a hitherto unknown factor(s) in the cellular milieu.

CONCLUSIONS

Here, we investigated the consequences of UHMK1 phosphorylation of a conserved SPSP motif of human SF1 for two major classes of interactions: protein-protein interactions with UHM-containing splicing factors and protein-RNA interactions for recognition of the 3′ splice site. First, we confirmed that phosphorylation slightly enhances the binding affinity of SF1 for its cognate UHM partner, $U2AF^{65}$. We further showed that UHMK1 phosphorylation slightly reduces binding of phospho-SF1 to other UHMs

that are unlikely to participate in functional heterodimers, including SPF45, U2AF^{35}, and CAPERα. Altogether, the net effect of phosphorylation is to subtly promote SF1 binding to U2AF^{65} and disfavor off-target complexes with other UHMs. Next, we quantified the influence of the UHMK1-phosphorylated SPSP motif on SF1 binding to splice-site RNAs. Regardless of the experimental context, including ITC or fluorescence anisotropy methods and the sequence of the splice-site RNA (AdML or suboptimal BPS variants of U6 or B3P3 RNAs), we found that phosphorylation by UHMK1 consistently but subtly reduced the affinities of SF1 or the SF1-U2AF^{65} complex for binding splice-site RNAs. Replacement of the SF1 coiled-coil domain for an unrelated domain from Staphylococcal protein A, or mutations of arginine residues surrounding the phosphorylated serines, reduced the affinities of SF1 or the SF1-U2AF^{65} complex for binding a representative, B3P3$_{\mathrm{SUBOPT}}$ RNA, which suggests that this SF1 region functions in 3′-splice-site recognition. Moreover, we show that the SF1 coiled coil and arginine residues of the SPSP-containing loop contribute to cooperative RNA recognition by the SF1-U2AF^{65} complex, and that SPSP phosphorylation reduces this cooperativity. The relatively subtle effects of SPSP-motif phosphorylation on SF1 binding affinities for UHM-containing splicing factors or RNA is likely to be significant at intracellular levels of SF1. Nonetheless, considering that the SF1 SPSP motif is predominately phosphorylated in proliferating cells and is essential for cell proliferation, comprehensive investigations of the potential functions of SF1 SPSP phosphorylation should be pursued in the near future.

SUPPORTING MATERIAL

Six figures and one table are available at http://www.biophysj.org/biophysj/supplemental/S0006-3495(16)31034-7.

AUTHOR CONTRIBUTIONS

R.C. accomplished the fluorescence anisotropy assays and ITC experiments. W.W., A.G., and S.L. accomplished additional ITC experiments. C.L.K. designed the research and wrote the paper with input from A.M., R.C., W.W., and A.G.

ACKNOWLEDGMENTS

We thank Dr. B. Miller, A. Grossfield, J. Jenkins, S. Messing and her colleagues in the Biostatistics department for constructive discussions of our data and analysis.

This work was supported by a National Institutes of Health grant (no. R01 GM070503).

REFERENCES

1. Abovich, N., and M. Rosbash. 1997. Cross-intron bridging interactions in the yeast commitment complex are conserved in mammals. *Cell.* 89:403–412.
2. Rutz, B., and B. Séraphin. 2000. A dual role for BBP/ScSF1 in nuclear pre-mRNA retention and splicing. *EMBO J.* 19:1873–1886.
3. Mazroui, R., A. Puoti, and A. Krämer. 1999. Splicing factor SF1 from *Drosophila* and *Caenorhabditis*: presence of an N-terminal RS domain and requirement for viability. *RNA.* 5:1615–1631.
4. Tanackovic, G., and A. Krämer. 2005. Human splicing factor SF3a, but not SF1, is essential for pre-mRNA splicing *in vivo*. *Mol. Biol. Cell.* 16:1366–1377.
5. Toda, T., A. Iida, …, T. Imai. 1994. Isolation and characterization of a novel gene encoding nuclear protein at a locus (D11S636) tightly linked to multiple endocrine neoplasia type 1 (MEN1). *Hum. Mol. Genet.* 3:465–470.
6. Rino, J., J. M. Desterro, …, M. Carmo-Fonseca. 2008. Splicing factors SF1 and U2AF associate in extraspliceosomal complexes. *Mol. Cell. Biol.* 28:3045–3057.
7. Berglund, J. A., N. Abovich, and M. Rosbash. 1998. A cooperative interaction between U2AF^{65} and mBBP/SF1 facilitates branchpoint region recognition. *Genes Dev.* 12:858–867.
8. Rudner, D. Z., R. Kanaar, …, D. C. Rio. 1998. Interaction between subunits of heterodimeric splicing factor U2AF is essential in vivo. *Mol. Cell. Biol.* 18:1765–1773.
9. Golling, G., A. Amsterdam, …, N. Hopkins. 2002. Insertional mutagenesis in zebrafish rapidly identifies genes essential for early vertebrate development. *Nat. Genet.* 31:135–140.
10. Yoshida, K., M. Sanada, …, S. Ogawa. 2011. Frequent pathway mutations of splicing machinery in myelodysplasia. *Nature.* 478:64–69.
11. Graubert, T. A., D. Shen, …, M. J. Walter. 2011. Recurrent mutations in the U2AF1 splicing factor in myelodysplastic syndromes. *Nat. Genet.* 44:53–57.
12. Makishima, H., V. Visconte, …, J. P. Maciejewski. 2012. Mutations in the spliceosome machinery, a novel and ubiquitous pathway in leukemogenesis. *Blood.* 119:3203–3210.
13. Matera, A. G., and Z. Wang. 2014. A day in the life of the spliceosome. *Nat. Rev. Mol. Cell Biol.* 15:108–121.
14. Berglund, J. A., K. Chua, …, M. Rosbash. 1997. The splicing factor BBP interacts specifically with the pre-mRNA branchpoint sequence UACUAAC. *Cell.* 89:781–787.
15. Zamore, P. D., J. G. Patton, and M. R. Green. 1992. Cloning and domain structure of the mammalian splicing factor U2AF. *Nature.* 355:609–614.
16. Wu, S., C. M. Romfo, …, M. R. Green. 1999. Functional recognition of the 3′ splice site AG by the splicing factor U2AF^{35}. *Nature.* 402:832–835.
17. Zorio, D. A., and T. Blumenthal. 1999. Both subunits of U2AF recognize the 3′ splice site in *Caenorhabditis elegans*. *Nature.* 402:835–838.
18. Merendino, L., S. Guth, …, J. Valcárcel. 1999. Inhibition of msl-2 splicing by Sex-lethal reveals interaction between U2AF^{35} and the 3′ splice site AG. *Nature.* 402:838–841.
19. Becerra, S., M. Montes, …, C. Suñé. 2015. Prp40 pre-mRNA processing factor 40 homolog B (PRPF40B) associates with SF1 and U2AF65 and modulates alternative pre-mRNA splicing in vivo. *RNA.* 21: 438–457.
20. Schwer, B., J. Chang, and S. Shuman. 2013. Structure-function analysis of the 5′ end of yeast U1 snRNA highlights genetic interactions with the Msl5*Mud2 branchpoint-binding complex and other spliceosome assembly factors. *Nucleic Acids Res.* 41:7485–7500.
21. Chang, J., B. Schwer, and S. Shuman. 2012. Structure-function analysis and genetic interactions of the yeast branchpoint binding protein Msl5. *Nucleic Acids Res.* 40:4539–4552.
22. Gozani, O., J. Potashkin, and R. Reed. 1998. A potential role for U2AF-SAP 155 interactions in recruiting U2 snRNP to the branch site. *Mol. Cell. Biol.* 18:4752–4760.
23. Thickman, K. R., M. C. Swenson, …, C. L. Kielkopf. 2006. Multiple U2AF^{65} binding sites within SF3b155: thermodynamic and spectroscopic characterization of protein-protein interactions among pre-mRNA splicing factors. *J. Mol. Biol.* 356:664–683.

24. Cass, D. M., and J. A. Berglund. 2006. The SF3b155 N-terminal domain is a scaffold important for splicing. *Biochemistry.* 45:10092–10101.

25. Spadaccini, R., U. Reidt, …, M. Sattler. 2006. Biochemical and NMR analyses of an SF3b155-p14-U2AF-RNA interaction network involved in branch point definition during pre-mRNA splicing. *RNA.* 12:410–425.

26. Haraguchi, N., T. Andoh, …, T. Tani. 2007. Mutations in the SF1-U2AF59-U2AF23 complex cause exon skipping in *Schizosaccharomyces pombe*. *J. Biol. Chem.* 282:2221–2228.

27. Shitashige, M., Y. Naishiro, …, T. Yamada. 2007. Involvement of splicing factor-1 in β-catenin/T-cell factor-4-mediated gene transactivation and pre-mRNA splicing. *Gastroenterology.* 132:1039–1054.

28. Corioni, M., N. Antih, …, A. Krämer. 2011. Analysis of in situ pre-mRNA targets of human splicing factor SF1 reveals a function in alternative splicing. *Nucleic Acids Res.* 39:1868–1879.

29. Jang, Y. H., H. Y. Park, …, J. K. Kim. 2014. A homolog of splicing factor SF1 is essential for development and is involved in the alternative splicing of pre-mRNA in *Arabidopsis thaliana*. *Plant J.* 78:591–603.

30. Rutz, B., and B. Séraphin. 1999. Transient interaction of BBP/ScSF1 and Mud2 with the splicing machinery affects the kinetics of spliceosome assembly. *RNA.* 5:819–831.

31. Guth, S., and J. Valcárcel. 2000. Kinetic role for mammalian SF1/BBP in spliceosome assembly and function after polypyrimidine tract recognition by U2AF. *J. Biol. Chem.* 275:38059–38066.

32. Zhang, D., A. J. Paley, and G. Childs. 1998. The transcriptional repressor ZFM1 interacts with and modulates the ability of EWS to activate transcription. *J. Biol. Chem.* 273:18086–18091.

33. Zhang, D., and G. Childs. 1998. Human ZFM1 protein is a transcriptional repressor that interacts with the transcription activation domain of stage-specific activator protein. *J. Biol. Chem.* 273:6868–6877.

34. Rain, J. C., and P. Legrain. 1997. In vivo commitment to splicing in yeast involves the nucleotide upstream from the branch site conserved sequence and the Mud2 protein. *EMBO J.* 16:1759–1771.

35. Wang, Q., L. Zhang, …, B. C. Rymond. 2008. A BBP-Mud2p heterodimer mediates branchpoint recognition and influences splicing substrate abundance in budding yeast. *Nucleic Acids Res.* 36:2787–2798.

36. Takemura, R., T. Takeiwa, …, M. Ohno. 2011. Multiple factors in the early splicing complex are involved in the nuclear retention of pre-mRNAs in mammalian cells. *Genes Cells.* 16:1035–1049.

37. Selenko, P., G. Gregorovic, …, M. Sattler. 2003. Structural basis for the molecular recognition between human splicing factors $U2AF^{65}$ and SF1/mBBP. *Mol. Cell.* 11:965–976.

38. Kielkopf, C. L., N. A. Rodionova, …, S. K. Burley. 2001. A novel peptide recognition mode revealed by the x-ray structure of a core $U2AF^{35}$/$U2AF^{65}$ heterodimer. *Cell.* 106:595–605.

39. Kielkopf, C. L., S. Lücke, and M. R. Green. 2004. U2AF homology motifs: protein recognition in the RRM world. *Genes Dev.* 18:1513–1526.

40. Loerch, S., A. Maucuer, …, C. L. Kielkopf. 2014. Cancer-relevant splicing factor CAPERα engages the essential splicing factor SF3b155 in a specific ternary complex. *J. Biol. Chem.* 289:17325–17337.

41. Corsini, L., S. Bonnal, …, M. Sattler. 2007. U2AF-homology motif interactions are required for alternative splicing regulation by SPF45. *Nat. Struct. Mol. Biol.* 14:620–629.

42. Wang, W., A. Maucuer, …, C. L. Kielkopf. 2013. Structure of phosphorylated SF1 bound to $U2AF^{65}$ in an essential splicing factor complex. *Structure.* 21:197–208.

43. Zhang, Y., T. Madl, …, M. Sattler. 2013. Structure, phosphorylation and U2AF65 binding of the N-terminal domain of splicing factor 1 during 3′-splice site recognition. *Nucleic Acids Res.* 41:1343–1354.

44. Wang, X., S. Bruderer, …, P. J. Robinson. 1999. Phosphorylation of splicing factor SF1 on Ser20 by cGMP-dependent protein kinase regulates spliceosome assembly. *EMBO J.* 18:4549–4559.

45. de Chiara, C., R. P. Menon, …, A. Pastore. 2009. Phosphorylation of S776 and 14-3-3 binding modulate ataxin-1 interaction with splicing factors. *PLoS One.* 4:e8372.

46. Manceau, V., M. Swenson, …, A. Maucuer. 2006. Major phosphorylation of SF1 on adjacent Ser-Pro motifs enhances interaction with $U2AF^{65}$. *FEBS J.* 273:577–587.

47. Lipp, J. J., M. C. Marvin, …, C. Guthrie. 2015. SR protein kinases promote splicing of nonconsensus introns. *Nat. Struct. Mol. Biol.* 22:611–617.

48. Manceau, V., E. Kremmer, …, A. Maucuer. 2012. The protein kinase KIS impacts gene expression during development and fear conditioning in adult mice. *PLoS One.* 7:e43946.

49. Manceau, V., C. L. Kielkopf, …, A. Maucuer. 2008. Different requirements of the kinase and UHM domains of KIS for its nuclear localization and binding to splicing factors. *J. Mol. Biol.* 381:748–762.

50. Maucuer, A., J. P. Le Caer, …, A. Sobel. 2000. Specific Ser-Pro phosphorylation by the RNA-recognition motif containing kinase KIS. *Eur. J. Biochem.* 267:4456–4464.

51. Wiseman, T., S. Williston, …, L. N. Lin. 1989. Rapid measurement of binding constants and heats of binding using a new titration calorimeter. *Anal. Biochem.* 179:131–137.

52. Jenkins, J. L., H. Shen, …, C. L. Kielkopf. 2008. Solution conformation and thermodynamic characteristics of RNA binding by the splicing factor $U2AF^{65}$. *J. Biol. Chem.* 283:33641–33649.

53. Okeyo-Owuor, T., B. S. White, …, T. A. Graubert. 2015. U2AF1 mutations alter sequence specificity of pre-mRNA binding and splicing. *Leukemia.* 29:909–917.

54. de Winter, J. C. F. 2013. Using the Student's t-test with extremely small sample sizes. *Pract. Assess. Res. Eval.* 18. Available online: http://pareonline.net/getvn.asp?v=18&n=10.

55. Gupta, A., J. L. Jenkins, and C. L. Kielkopf. 2011. RNA induces conformational changes in the SF1/$U2AF^{65}$ splicing factor complex. *J. Mol. Biol.* 405:1128–1138.

56. Agrawal, A. A., E. Salsi, …, C. L. Kielkopf. 2016. An extended $U2AF^{65}$-RNA-binding domain recognizes the 3′ splice site signal. *Nat. Commun.* 7:10950.

57. Mullen, M. P., C. W. Smith, …, B. Nadal-Ginard. 1991. Alpha-tropomyosin mutually exclusive exon selection: competition between branchpoint/polypyrimidine tracts determines default exon choice. *Genes Dev.* 5:642–655.

58. Peled-Zehavi, H., J. A. Berglund, …, A. D. Frankel. 2001. Recognition of RNA branch point sequences by the KH domain of splicing factor 1 (mammalian branch point binding protein) in a splicing factor complex. *Mol. Cell. Biol.* 21:5232–5241.

59. McLaughlin, K. J., J. L. Jenkins, and C. L. Kielkopf. 2011. Large favorable enthalpy changes drive specific RNA recognition by RNA recognition motif proteins. *Biochemistry.* 50:1429–1431.

60. Fukada, H., and K. Takahashi. 1998. Enthalpy and heat capacity changes for the proton dissociation of various buffer components in 0.1 M potassium chloride. *Proteins.* 33:159–166.

61. Gao, Q., I. Mechin, …, S. M. Huang. 2013. Evaluation of cancer dependence and druggability of PRP4 kinase using cellular, biochemical, and structural approaches. *J. Biol. Chem.* 288:30125–30138.

62. Hellman, L. M., and M. G. Fried. 2007. Electrophoretic mobility shift assay (EMSA) for detecting protein-nucleic acid interactions. *Nat. Protoc.* 2:1849–1861.

63. Taggart, A. J., A. M. DeSimone, …, W. G. Fairbrother. 2012. Large-scale mapping of branchpoints in human pre-mRNA transcripts in vivo. *Nat. Struct. Mol. Biol.* 19:719–721.

64. Mercer, T. R., M. B. Clark, …, J. S. Mattick. 2015. Genome-wide discovery of human splicing branchpoints. *Genome Res.* 25:290–303.

65. Liu, Z., I. Luyten, …, M. Sattler. 2001. Structural basis for recognition of the intron branch site RNA by splicing factor 1. *Science.* 294:1098–1102.

66. Jacewicz, A., L. Chico, …, S. Shuman. 2015. Structural basis for recognition of intron branchpoint RNA by yeast Msl5 and selective effects of

interfacial mutations on splicing of yeast pre-mRNAs. *RNA.* 21:401–414.

67. Mackereth, C. D., T. Madl, …, M. Sattler. 2011. Multi-domain conformational selection underlies pre-mRNA splicing regulation by U2AF. *Nature*. 475:408–411.

68. Wang, C., K. Chua, …, R. Reed. 1998. Phosphorylation of spliceosomal protein SAP 155 coupled with splicing catalysis. *Genes Dev.* 12:1409–1414.

69. Tanuma, N., S. E. Kim, …, H. Shima. 2008. Nuclear inhibitor of protein phosphatase-1 (NIPP1) directs protein phosphatase-1 (PP1) to dephosphorylate the U2 small nuclear ribonucleoprotein particle (snRNP) component, spliceosome-associated protein 155 (Sap155). *J. Biol. Chem.* 283:35805–35814.

70. Zhou, Z., and X. D. Fu. 2013. Regulation of splicing by SR proteins and SR protein-specific kinases. *Chromosoma.* 122:191–207.

71. Wang, H. Y., W. Lin, …, X. D. Fu. 1998. SRPK2: a differentially expressed SR protein-specific kinase involved in mediating the interaction and localization of pre-mRNA splicing factors in mammalian cells. *J. Cell Biol.* 140:737–750.

72. Chen, H. K., P. Fernandez-Funez, …, H. Y. Zoghbi. 2003. Interaction of Akt-phosphorylated ataxin-1 with 14-3-3 mediates neurodegeneration in spinocerebellar ataxia type 1. *Cell.* 113:457–468.

Biophysical Journal, Volume *111*

Supplemental Information

SF1 Phosphorylation Enhances Specific Binding to U2AF^{65} and Reduces Binding to 3′-Splice-Site RNA

Rakesh Chatrikhi, Wenhua Wang, Ankit Gupta, Sarah Loerch, Alexandre Maucuer, and Clara L. Kielkopf

Supplementary Tables

Table S1. Thermodynamics of SF1 binding $U2AF^{65}$ proteins in different ionic strengths.[a]

Interaction:	**K_D** (nM)	**ΔG**[b] (kcal mol^{-1})	**ΔH** (kcal mol^{-1})	**$-T\Delta S$**[c] (kcal mol^{-1})	**n**[d]
$U2AF^{65}_{R12U}$ in 100 mM NaCl buffer titrated into: [e]					
$SF1_{1-255}$	60 ± 5	-10.1 ± 0.1	-13.5 ± 0.5	3.5 ± 0.1	1.0 ± 0.1
Phospho-$SF1_{1-255}$	40 ± 12	-10.3 ± 0.2	-14.5 ± 0.2	4.2 ± 0.1	0.9 ± 0.1
$U2AF^{65}$ UHM in 100 mM NaCl buffer titrated into: [f,g]					
$SF1_{14-132}$	43 ± 1	-10.2 ± 0.1	-13.5 ± 0.1	3.3 ± 0.1	1.0 ± 0.1
Phospho-$SF1_{14-132}$	24 ± 1	-10.6 ± 0.1	-20.6 ± 0.1	10.0 ± 0.1	0.9 ± 0.1
$U2AF^{65}$ UHM in 250 mM NaCl buffer titrated into: [f]					
$SF1_{14-132}$	940 ± 47	-8.4 ± 0.1	-13.5 ± 0.5	5.1 ± 0.5	0.9 ± 0.1
Phospho-$SF1_{14-132}$	623 ± 20	-8.6 ± 0.1	-14.5 ± 0.1	5.8 ± 0.1	1.0 ± 0.1

[a] Average values and standard deviations of at least two independent titrations.
[b] Calculated using the equation $\Delta G = -RT \ln (K_D^{-1})$ at T=303 K.
[c] Calculated using the equation $-T\Delta S = \Delta G - \Delta H$.
[d] Apparent stoichiometry of $U2AF^{65}$:SF1 proteins (n).
[e] $c = [M]/K_D$ where [M] is the concentration of macromolecule in the sample cell.
[f] 100 mM NaCl and 250 mM NaCl buffers include 25 mM HEPES pH 7.4, 0.2 mM TCEP.
[g] Also shown for comparison in Table 1.

Supplementary Figures

Figure S1. Control titrations of proteins or RNA into buffer, including (**A**) SPF45 UHM (200 μM), (**B**) U2AF^{35} UHM (200 μM), (**C**) 35 μM B3P3 RNA, or (**D**) 35 μM SF1$_{1\text{-}255}$ – U2AF$^{65}_{R12U}$ complex. The control titration of CAPERα UHM into buffer is shown in Loerch *et al*. (2014) *J. Biol. Chem*. 289:17325-17337.

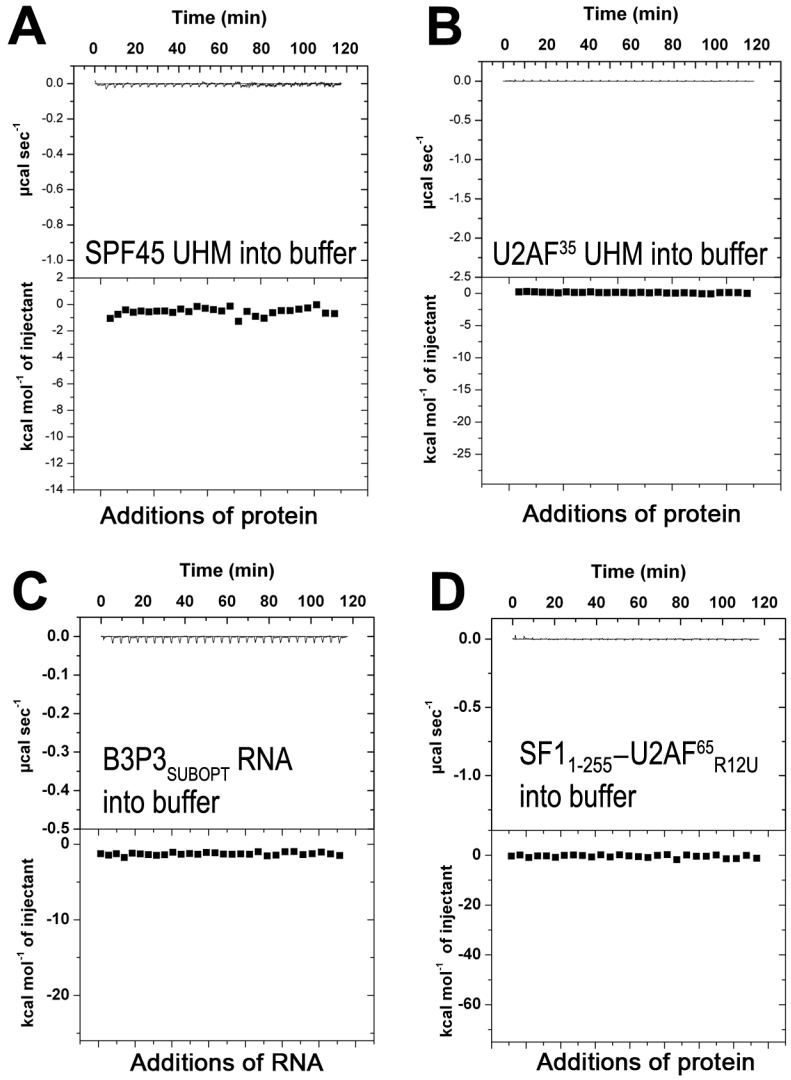

Figure S2. Representative isotherms of SF1 or phospho-SF1 titrated with U2AF^{65} constructs and fit with identical sites binding models. The buffer in (**A-B**) is 100 mM NaCl, 25 mM HEPES pH 7.4, 0.2 mM TCEP. The titrations include (**A**) 48 μM U2AF$^{65}{}_{R12U}$ into 6 μM SF1$_{1-255}$, c=100. (**B**) 32 μM U2AF$^{65}{}_{R12U}$ into 4 μM phospho-SF1$_{1-255}$, c=100. The buffer in (**C-D**) is 250 mM NaCl, 25 mM HEPES pH 7.4, 0.2 mM TCEP. The titrations include (**C**) 120 μM U2AF^{65} UHM into 15 μM SF1$_{14-132}$, c=16. (**D**) 120 μM U2AF^{65} UHM into 15 μM phospho-SF1$_{14-132}$, c=24. The apparent equilibrium dissociation constants (K_D) and standard deviations between two titrations are given.

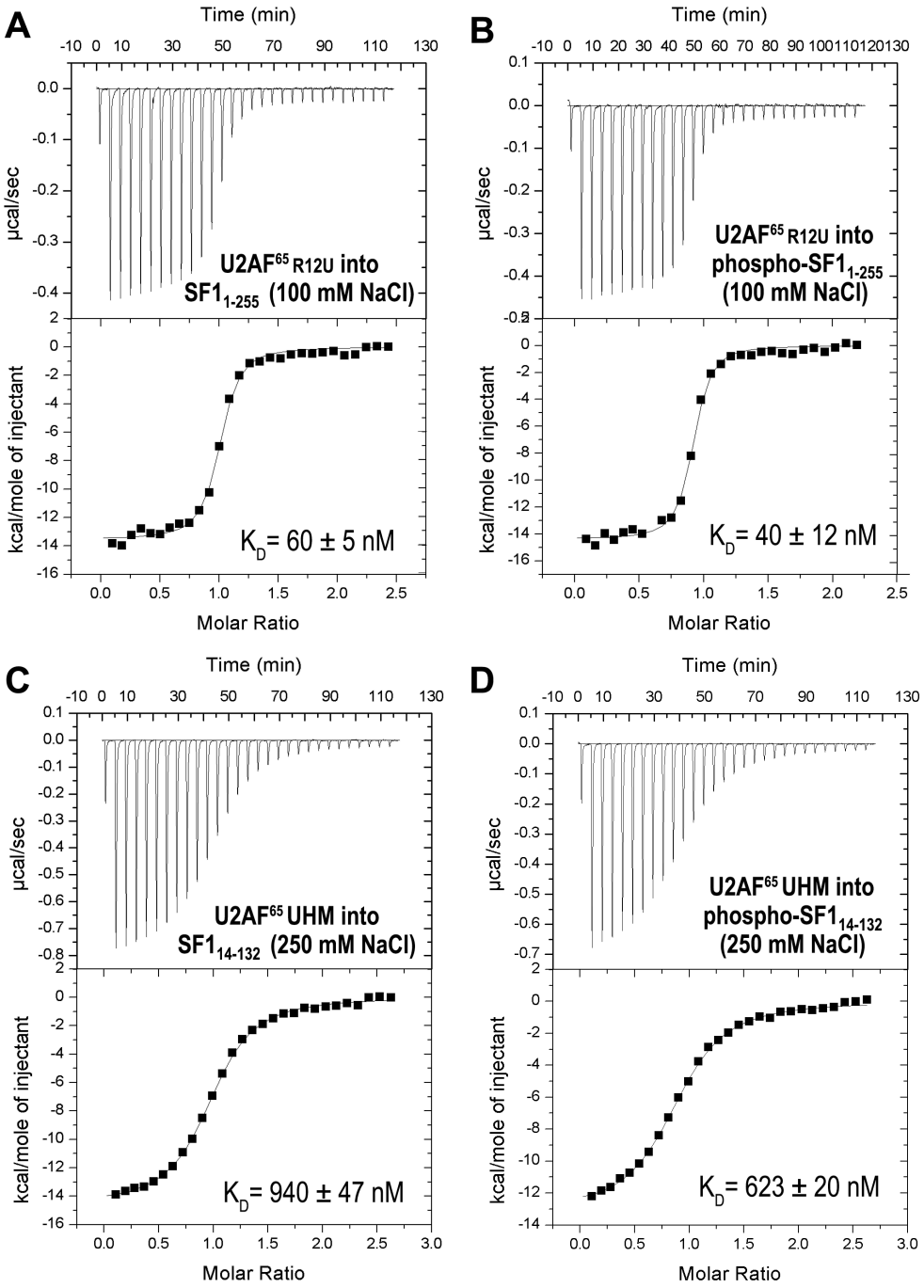

Figure S3. Schematic diagram of binding events during the titration of $SF1_{1\text{-}255}$ or phospho-$SF1_{1\text{-}255}$ into a mixture of $U2AF^{65}$ (or $U2AF^{65}$–$U2AF^{35}$ UHM complex) and fluorescein-labeled AdML RNA, for which apparent K_D's are given in Figure 3. A dashed line separates the titrated $SF1_{1\text{-}255}$ or phospho-$SF1_{1\text{-}255}$ proteins from the mixture in the cuvette. Based on the ~30 nM K_D of the full length $U2AF^{65}$–$U2AF^{35}$ UHM complex binding the AdML Py tract (56) and a 25 nM concentration of $U2AF^{65}$–$U2AF^{35}$ UHM protein and RNA in the sample cell, approximately 8 nM $U2AF^{65}$–$U2AF^{35}$ UHM–RNA complex and 17 nM free $U2AF^{65}$–$U2AF^{35}$ UHM protein and RNA are present in the sample cell at the start of the titration. The K_D's of other binding reactions are not known for the current constructs, RNA sequence, ionic strength, and pH.

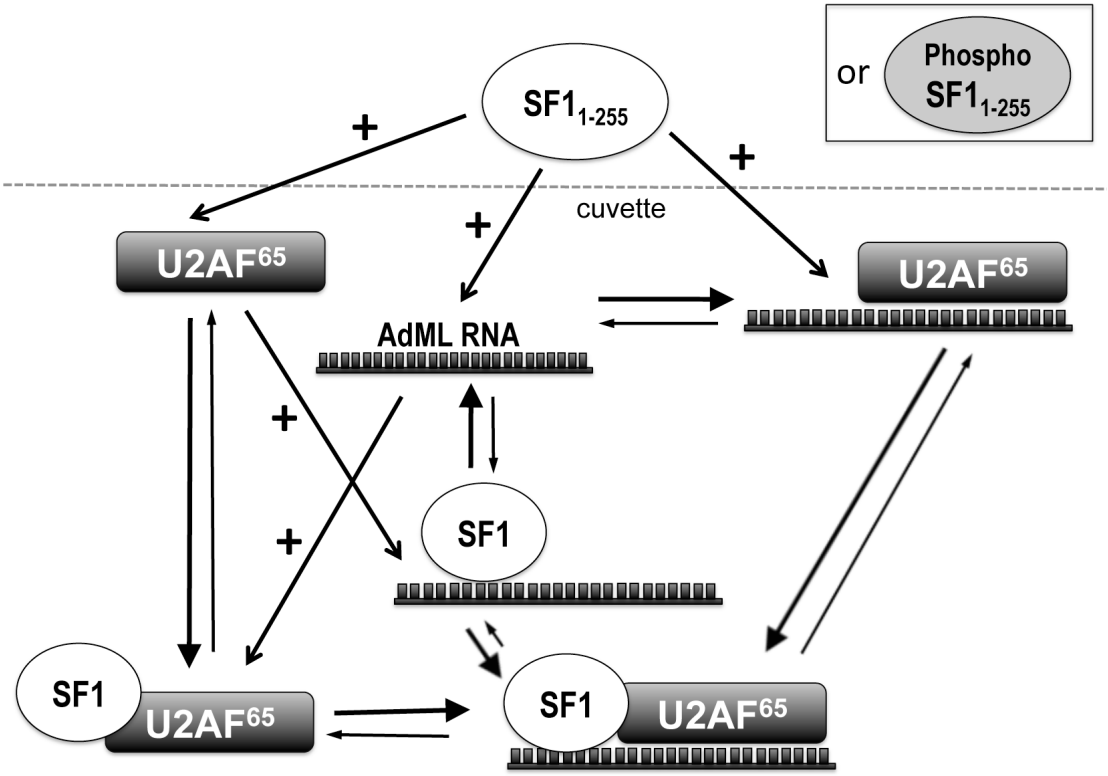

Figure S4. Representative isotherm showing 100 μM B3P3 RNA titrated into 5 μM $U2AF^{65}{}_{R12U}$ (c=10) and fit with an identical sites binding model. The apparent equilibrium dissociation constant (K_D) and standard deviation between two titrations is given.

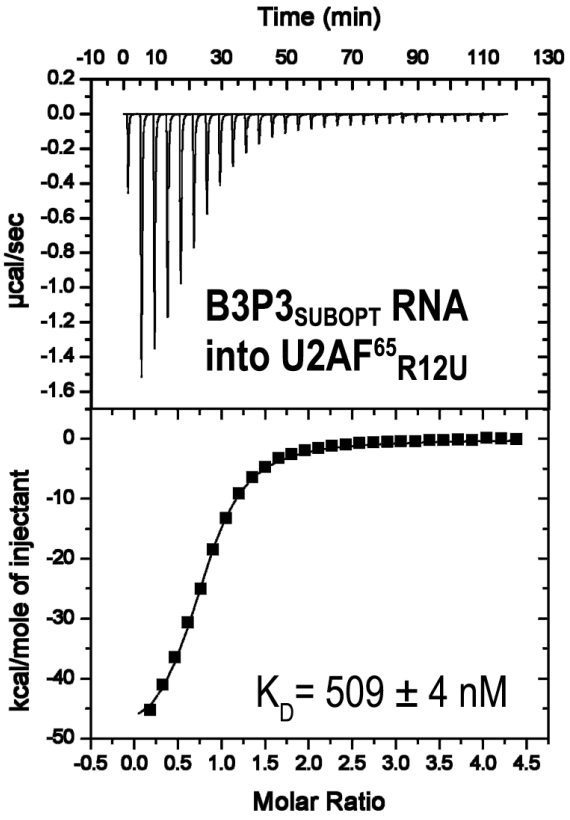

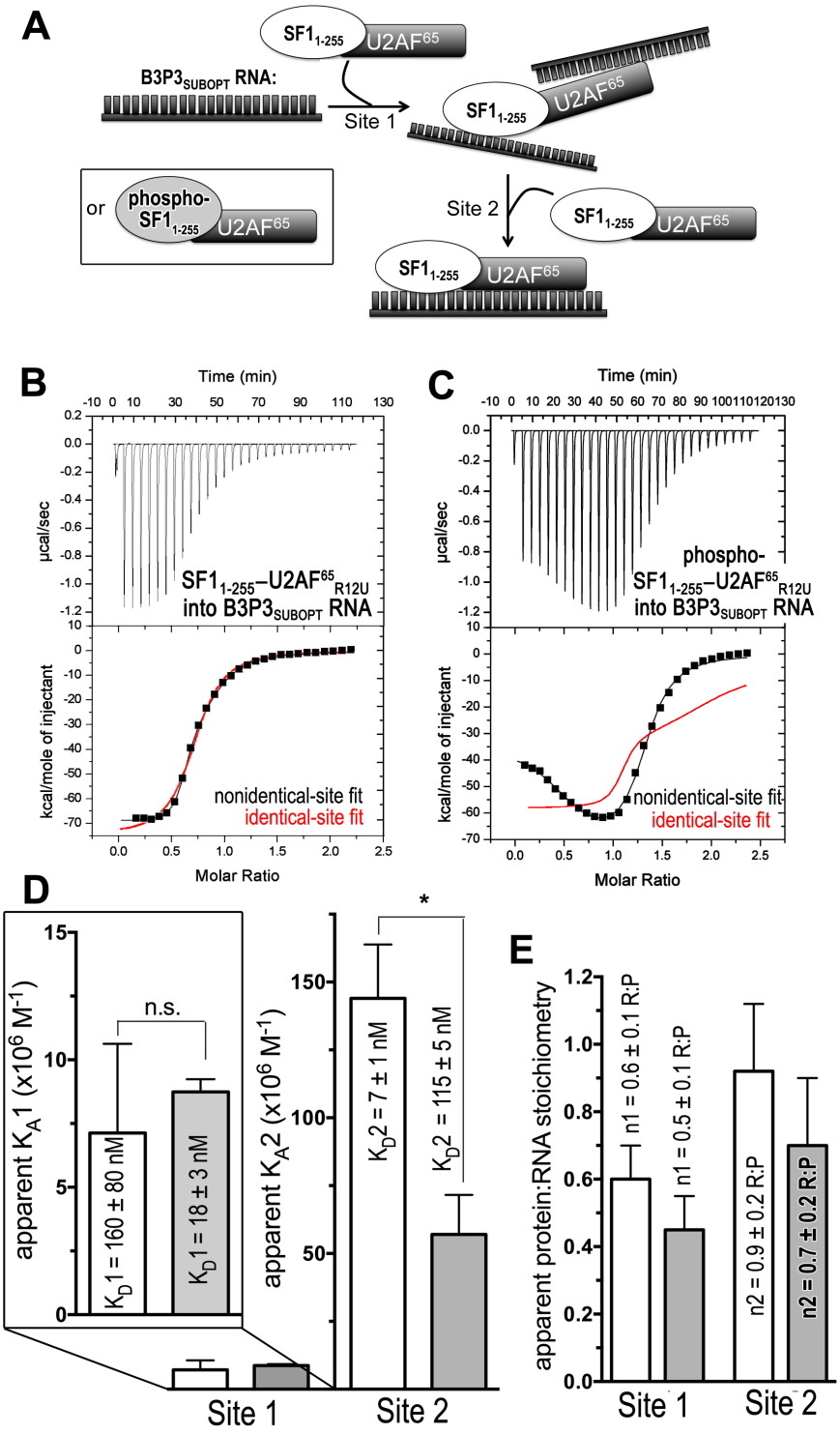

Figure S5. ITC results for $SF1_{1\text{-}255}$ – $U2AF^{65}{}_{R12U}$ or phospho-$SF1_{1\text{-}255}$ – $U2AF^{65}{}_{R12U}$ reverse titrated into B3P3 RNA. (**A**) Schematic diagram of the ITC experiment. (**B**-**C**) Representative isotherms fit with binding models for either nonidentical sites (black lines) or identical sites (red lines). (**B**) 35 μM $SF1_{1\text{-}255}$ – $U2AF^{65}{}_{R12U}$ complex into 5 μM B3P3 RNA (nonidentical site χ^2= 0.30E6 ± 0.20E6; identical sites χ^2 = 1.88E6 ± 0.69E6), c=31 for site 1 and c=714 for site 2. (**C**) 50 μM phospho-$SF1_{1\text{-}255}$ – $U2AF^{65}{}_{R12U}$ complex into 5 μM B3P3 RNA (nonidentical sites (χ^2 = 1.45E6 ± 0.14E6; identical sites χ^2 = 82.3E6 ± 76.0E6), c=43 for site 1 and c=278 for site 2. The identical site models were discarded based on the large χ^2 increase and poor fit. (**D**) Bar graph of apparent affinities (K_A) of the interactions, colored as shown in (A). The apparent equilibrium dissociation constants (K_D) are given. An expanded view of the lower affinity sites is inset to the left. (**E**) Bar graph of apparent protein:RNA stoichiometries (n), colored as for (A).

Figure S6. Representative isotherm showing 50 μM $B3P3_{SUBOPT}$ RNA titrated into 5 μM SF1mut–$U2AF^{65}{}_{R12U}$ in 100 mM NaCl, 25 mM sodium phosphate pH 7.4. The isotherm was fit using an identical sites binding model. The apparent equilibrium dissociation constant (K_D) and standard deviation of two independent titrations is inset.